ANNUAL REVIEWS

Annual Review of Fluid Mechanics

Elasto-Inertial Turbulence

Yves Dubief,[1] Vincent E. Terrapon,[2] and Björn Hof[3]

[1]Department of Mechanical Engineering, University of Vermont, Burlington, Vermont, USA; email: ydubief@uvm.edu

[2]Department of Aerospace & Mechanical Engineering, University of Liège, Liège, Belgium

[3]Institute of Science and Technology Austria, Klosterneuburg, Austria

Annu. Rev. Fluid Mech. 2023. 55:675–705

First published as a Review in Advance on October 20, 2022

The *Annual Review of Fluid Mechanics* is online at fluid.annualreviews.org

https://doi.org/10.1146/annurev-fluid-032822-025933

Keywords

elasto-inertial turbulence, elastic turbulence, elastic instabilities, polymer drag reduction, coherent structures, transitional flows, numerical simulation, viscoelastic models

Abstract

The dissolution of minute concentration of polymers in wall-bounded flows is well-known for its unparalleled ability to reduce turbulent friction drag. Another phenomenon, elasto-inertial turbulence (EIT), has been far less studied even though elastic instabilities have already been observed in dilute polymer solutions before the discovery of polymer drag reduction. EIT is a chaotic state driven by polymer dynamics that is observed across many orders of magnitude in Reynolds number. It involves energy transfer from small elastic scales to large flow scales. The investigation of the mechanisms of EIT offers the possibility to better understand other complex phenomena such as elastic turbulence and maximum drag reduction. In this review, we survey recent research efforts that are advancing the understanding of the dynamics of EIT. We highlight the fundamental differences between EIT and Newtonian/inertial turbulence from the perspective of experiments, numerical simulations, instabilities, and coherent structures. Finally, we discuss the possible links between EIT and elastic turbulence and polymer drag reduction, as well as the remaining challenges in unraveling the self-sustaining mechanism of EIT.

1. INTRODUCTION

EIT: elasto-inertial turbulence

ET: elastic turbulence

IT: inertial turbulence

MDR: maximum drag reduction

The dynamical state of elasto-inertial turbulence (EIT) has been defined only rather recently (Samanta et al. 2013), and the extent of its prevalence in viscoelastic flows is not yet fully established and is subject to ongoing investigation. As the name implies, the distinguishing feature of EIT is that disordered motion arises from both inertial forces and elastic stresses, in opposition to elastic turbulence (ET), which is a chaotic regime (CR) caused by elastic stresses in inertialess flows (Steinberg 2021). The instability that gives rise to EIT is distinct from the transition to inertial turbulence (IT) (Reynolds 1883, Avila et al. 2023) and features qualitatively different structures (spanwise instead of streamwise coherent structures) and a different self-sustaining mechanism. Yet across a large parameter range of Reynolds number and viscoelastic parameters, EIT and IT coexist, which complicates the distinction between these two chaotic flow states and in part explains the late (re)discovery of EIT. The first observations of turbulent-like motions at unusually low Reynolds numbers (*Re*) in viscoelastic fluids date back to the early twentieth century (Ostwald & Auerbach 1926). In contrast to Newtonian pipe flow, where turbulence only sets in for $Re \sim 2{,}000$ and higher, these studies reported that in dilute aqueous polymer solutions, so-called early turbulence can already arise at *Re* of order one. Subsequently, little attention has been paid to these studies, and instead the main focus has been on the seemingly unrelated phenomenon of polymer drag reduction (i.e., the quasi-suppression of IT by the addition of small amounts of polymers to Newtonian solvents). It is noteworthy that, in the context of drag reduction, studies reported a transition delay, in contrast to the abovementioned phenomenon of early turbulence.

Early turbulence finally regained attention when two independent studies, one numerical (Dubief et al. 2010, Dubief & White 2011) and the other experimental (Hof et al. 2011), found evidence for novel flow structures, on the one hand, and for a distinct transition branch, on the other. The former study reported results of direct numerical simulations (DNS) using a constitutive model to capture the dynamics of dilute polymer solutions. In the so-called maximum drag reduction (MDR) limit, the authors discovered structures distinct from Newtonian streaks and vortices (Dubief et al. 2010). The generation and sustenance of these structures were linked to elastic instabilities. The experimental study, on the other hand, exploited recent insights into the transition in Newtonian pipe flow and in doing so could distinguish between two competing instabilities, one requiring finite-amplitude perturbations and giving rise to Newtonian-type puffs, and the other, without hysteresis, giving rise to a globally fluctuating state, EIT. In agreement with the early turbulence literature, the latter state could be detected at *Re* well below 2,000. In addition, however, by exploiting the linear stability of Hagen–Poiseuille flow, this instability could be tracked to much higher *Re* ($\sim$5,000). Surprisingly, the friction factors detected (Samanta et al. 2013) above onset coincided with the MDR asymptote. Hence, EIT not only explains the moderate-inertia early turbulence phenomenon but also offers a new interpretation of the drag reduction limit in polymer solutions at large inertia.

Beyond its potential ability to modify mixing and drag at Reynolds numbers that would be laminar in the absence of polymers, EIT offers a unique window of investigation into the interactions between two dynamics (flow and polymers) at different scales. Specifically, chaos in EIT is the result of a backward energy transfer, from small scales to large scales, contrary to the well-accepted energy cascade of Newtonian turbulence, where energy flows toward increasingly small scales.

This review attempts to offer a comprehensive overview of the different approaches used to study EIT. It covers the challenges inherent to its numerical and experimental investigation and also provides our perspective on the research necessary to further advance understanding of EIT.

1.1. Polymer Drag Reduction

In pipe and channel flows of Newtonian fluids, the motion takes one of two forms: laminar at low Reynolds numbers and turbulent at high. This conceptual view, despite contrary evidence (see Section 5), has by and large also been adopted for pipe flow of complex viscoelastic fluids. The starting point of the Newtonian perspective applied to polymer flows was the discovery by Toms (1948) that the addition of a small quantity (typically a few ppm in weight) of long chain polymers to a turbulent flow can substantially reduce the drag. The effect of polymers on Newtonian turbulence and the underlying drag reduction mechanism have been studied in great detail following suggestions by Lumley (1969) of a viscous mechanism and a competing suggestion by Tabor & De Gennes (1986) of an elastic mechanism. For details regarding the polymer drag reduction mechanism, we refer the interested reader to the comprehensive reviews by White & Mungal (2008) and Xi (2019). In this context we would like to highlight several puzzling observations that could not be addressed by this classical approach, an approach that is strongly biased toward Newtonian turbulence and the modification of the underlying flow structures. While the amount of drag reduction is found to increase with polymer concentration, flows are normally not found to fully relaminarize. Instead a low fluctuation level persists and the corresponding drag approaches a well-defined limit, the so-called MDR asymptote (see **Figure 1*a***).

This drag limit turns out to be independent of the exact polymer solvent combination. Commonly used polymers in these studies are polyethyleneoxide, polyacrylamide, and polymethylmethacrylate with molecular weights in the range of millions of daltons, while concentrations range from a few to several hundred parts per million.

From the Newtonian turbulence perspective it is difficult to explain why the drag reduction falls short of relaminarizing flows, let alone why this limit should be universal. Frequently MDR has been interpreted as a marginal state of Newtonian turbulence, and some studies have connected

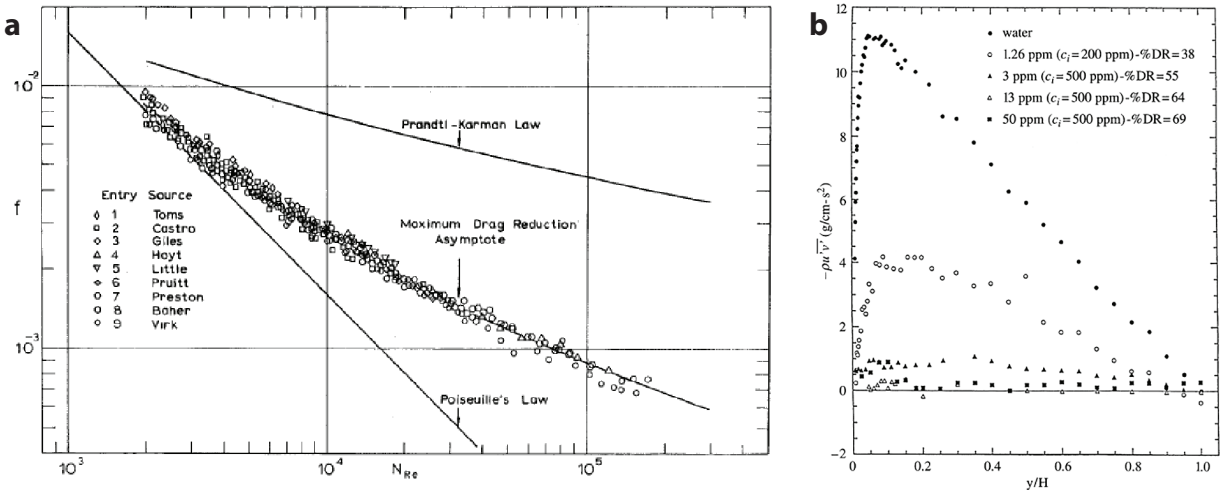

Figure 1

(*a*) Original friction factor plot of Virk et al. (1970). The graph shows the friction factor f as a function of the Reynolds number for a series of experiments (*symbols*). Lines define the laminar regime, Poiseuille's law, the maximum drag reduction (MDR) asymptote and the turbulent regime, the Prandtl–Karman law. Panel reprinted from Virk et al. (1970) with permission; copyright 1970 American Society of Mechanical Engineers. (*b*) Evolution of the Reynolds shear stress $-\rho\overline{u'v'}$ profiles as a function of the distance from the wall y normalized by the half-height of the channel H. Panel reprinted from Warholic et al. (1999) with permission; copyright 1999 Springer Nature.

it to the Newtonian edge state (Xi & Graham 2010). The edge state, however, is by definition unstable, and it is not a priori clear how polymers would turn it into a stable state. Another puzzling observation is that, in the MDR limit, Reynolds stresses are reduced by almost an order of magnitude (**Figure 1*b***). It is questionable whether Newtonian flow structures can be sustained at such low levels of Reynolds stress.

1.2. Early Turbulence Versus Transition Delay in Experiments

The discovery of turbulent-like fluctuations in polymer solutions at unusually low Reynolds numbers goes back to Ostwald & Auerbach (1926), who dubbed this phenomenon structural turbulence. It was subsequently noted by Reiner (1926a,b) that the onset of structural turbulence is determined by a critical shear rate, whereas the onset of IT is governed by the Reynolds number. Consequently, Reiner argues that the critical velocity for the onset of structural turbulence should be proportional to the ratio of the pipe radius and the fluid's molecular viscosity R/η, while the velocity threshold for IT is proportional to the inverse. The effect of the radius on the critical velocity for the onset of so-called Reynold's turbulence (IT), U_{krit}, and on the critical velocity for the onset of structural turbulence, V_{krit}, is illustrated in **Figure 2*a*** (Reiner 1926a). In agreement with this proposition, later experiments showed that in capillary tubes (i.e., for small R), structural turbulence could be pushed to Re as low as one (Ram & Tamir 1964). Moreover, it was noted by Little et al. (1975) that early turbulence causes a drag increase at low Reynolds

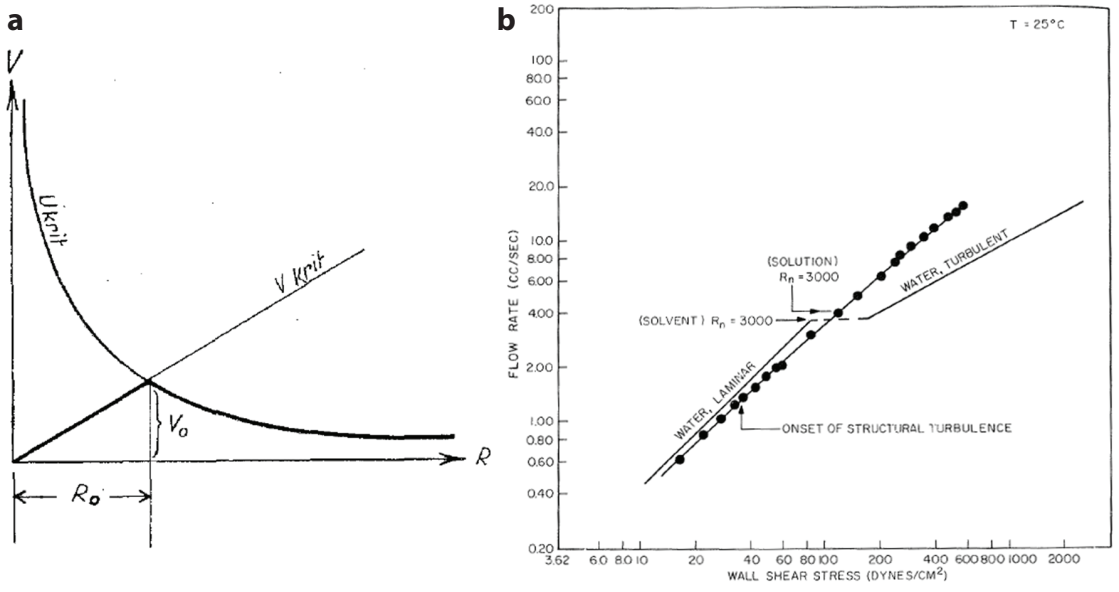

Figure 2

Structural turbulence. (*a*) From Reiner (1926b), a plot depicting the scaling of the transition threshold to Reynolds turbulence, U_{krit}, which scales with the inverse of the pipe radius R. V_{krit}, the transition threshold for structural turbulence, however, is proportional to the shear rate and hence increases linearly with radius. Panel reprinted from Reiner (1926b). (*b*) From Little & Wiegard (1970), a plot comparing the flow rate of a Newtonian solvent to that of a polymer solution. Starting from small wall shear stresses in both cases, the flow rates increase at the same rate up to the structural turbulence transition in the polymer solution. Structural turbulence causes higher drag; hence, the flow rate increases more slowly then the Newtonian case. This trend is reversed when the water flow becomes turbulent, resulting in substantially larger drag in the Newtonian solvent. Note that, in case of the polymer solution, after the onset of structural turbulence no further transition is observed. Panel reprinted from Little & Wiegard (1970) with permission; copyright 1970 John Wiley & Sons.

numbers (see **Figure 2*b***). The authors speculated about a common origin of the stabilizing drag reduction effect and the destabilizing early turbulence phenomenon. Later studies (e.g., Hoyt 1977) apparently did not distinguish between the two types of turbulence and, as a result, could not explain why some studies appeared to find a transition delay while others proposed an early transition: "Whether transition from laminar to turbulent flow is delayed in dilute polymer solutions, unchanged or occurs at an earlier Reynolds number has been a vexing question since research began in this area" (p. 508). Clearly, at that stage the studies of structural turbulence, its distinction as a separate dynamical state, and particularly the explanation offered by Reiner (1926a,b) on the opposing trends of the two instabilities had been forgotten. The early turbulence work suffered a similar fate since the focus of subsequent studies of polymer solutions shifted to the mechanism underlying drag reduction and took little note of the effect of polymers on transition.

1.3. Rediscovery of Elasto-Inertial Turbulence

The transition problem was finally revisited by Samanta et al. (2013), who applied recent insights gained in Newtonian fluids in an attempt to better quantify the effect of polymer additives. Since they initially focused on lifetimes of turbulent puffs, their study was carried out in a long, small-diameter tube, a setting where the onset of Newtonian turbulence is encountered at high shear rates and where, hence, the Weissenberg number is large.

A brief note on transition in Newtonian pipe flow is in order. In this case, the laminar Hagen–Poiseuille flow is linearly stable and turbulence can only arise from perturbations of finite amplitude (Reynolds 1883), a scenario often termed subcritical transition. The point where turbulence first arises in a given experiment, the natural transition point, is setup specific and depends on imperfections and disturbance levels. If, on the other hand, turbulence is initially triggered, for the timescales (i.e., pipe length) available in typical experiments, the onset of turbulence appears to depend on the perturbation used (e.g., orifice, periodic, or impulsive perturbation) (Mukund & Hof 2018). This apparent dependence on perturbation levels and on experimental details has made a characterization of the Newtonian turbulence transition difficult. At the same time, it has hindered quantitative studies of the effect of polymers on transition. Eventually progress in understanding of the Newtonian transition has allowed a quantitative and setup-independent characterization of turbulent puffs, the flow structures in the Newtonian transitional regime. In particular, the transient nature of puffs and the sensitive dependence of puff lifetimes (Hof et al. 2006, 2008) on control parameters make them ideal for detecting the effects of changes in fluid properties on transition. This sensitive dependence of puff lifetimes was exploited by Samanta et al. (2013) to determine the effect of polymer additives on transition and to discriminate the Newtonian turbulence transition from other dynamical states. The authors demonstrated that the subcritical transition to IT is delayed (see lower branch in **Figure 3**), in line with the drag reducing effect of polymers in turbulent flow. However, at higher shear rates a separate instability to a different fluctuating state was found (see upper branch with symbols and line in **Figure 3**). In this case, fluctuation levels were found to increase continuously with Re, not requiring any external perturbations. Moreover, unlike for Newtonian puffs, fluctuations arose globally throughout the flow. The fluctuation level, on the other hand, remained considerably lower than that in IT. In particular, these authors could follow the new branch (see **Figure 3**) to higher Reynolds numbers by avoiding the Newtonian transition (i.e., to inertial turbulence). Samanta et al. (2013) also observed that this transition was determined by a critical shear rate, unknowingly confirming the suggestion made by Reiner (1926a,b) 87 years earlier. Speculating that this shear-dependent turbulent state may be dynamically connected to a purely elastic instability that occurs in flows with

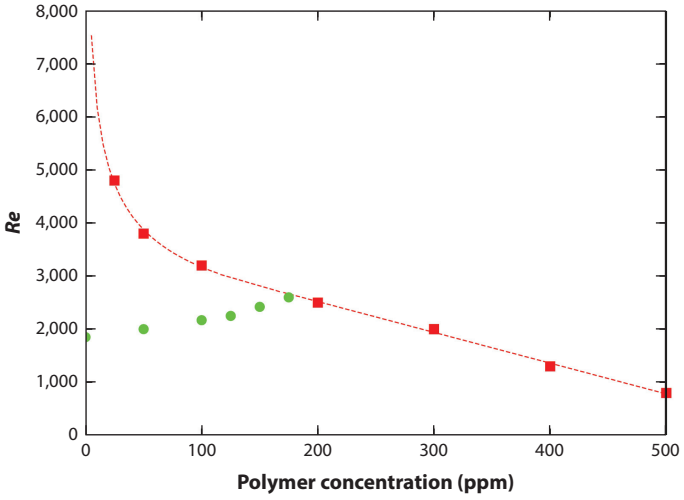

Figure 3

The transition threshold to Newtonian turbulence (*green points*, based on measurements of puff lifetimes) increases with polymer concentration. For larger polymer concentrations, however, a different instability branch (*red points*) marks the onset of elasto-inertial turbulence (EIT). By suppressing the subcritical transition to inertial turbulence, the EIT branch can be tracked to lower polymer concentrations. Figure adapted from Samanta et al. (2013) with permission; copyright 2013 the authors.

curved streamlines and, in particular, to the associated state of ET (Groisman & Steinberg 2000, Steinberg 2021), Samanta et al. (2013) dubbed this state "elasto-inertial turbulence." From an historical perspective, it is noteworthy that the term "elastic turbulence" was probably first used by Vinogradov & Manin (1965).

2. IMPORTANT LESSONS FROM NUMERICAL SIMULATIONS

Numerical simulations of viscoelastic flows have proven to be an essential tool in the study of EIT. They complement experiments by giving access to polymer dynamics, which is virtually impossible to measure at the macroscale of interest. However, the viscoelastic constitutive models and numerical methods they require suffer from limitations that can affect the simulated physics. Knowledge of these limitations and understanding of their influence on the dynamics of the flow are essential when studying the mechanisms of EIT, as such limitations can affect the simulated physics, but also some numerical limitations may be used to isolate key mechanisms of EIT. In this context, this section first introduces the most common general framework for viscoelastic DNS and then discusses best practices within the limitations of present computing power and numerical methods.

2.1. Constitutive Viscoelastic Models

This section focuses only on the most common models known for their ability to simulate EIT. A more detailed description of viscoelastic models may be found in the recent review by Alves et al. (2021). Here index tensorial notations are used and the Einstein index rule is implied unless stated otherwise.

Led by the pioneering work of Sureshkumar et al. (1997), the numerical community sought to understand polymer drag reduction using constitutive viscoelastic models. The tensor-transport

models Oldroyd-B and finitely extensible nonlinear elastic-Peterlin (FENE-P) (Bird et al. 1987) have been the most popular. Both may be described as follows. The flow is incompressible,

$$\partial_i u_i = 0, \tag{1.}$$

and governed by the Navier–Stokes equations supplemented by a viscoelastic stress T_{ij}:

$$\partial_t u_i + u_j \partial_j u_i = -\partial_i p + \frac{\beta}{Re}\partial_j \partial_j u_i + \frac{1-\beta}{Re}\partial_j T_{ij}\,. \tag{2.}$$

The parameter β is the ratio of the solvent viscosity to the zero-shear-rate viscosity of the polymer solution, and Re is the Reynolds number.

Individual polymer molecules are represented as two beads connected by a spring, also called the dumbbell model. The Lagrangian Brownian dynamics model of this simplified molecule is derived from the inertialess equilibrium between hydrodynamic forces (drag) on the beads, the spring or entropic force, and a Brownian term to account for the molecular thermal noise or interaction between the polymer molecule and the solvent molecules. This equation is expressed as a function of the end-to-end vector q_i connecting the two beads. At the continuum level, the local state of polymer molecules is reduced to the conformation tensor $C_{ij} = \langle q_i q_j \rangle$, where $\langle\cdot\rangle$ is the phase average over all local polymer molecules. Effectively the trace of this tensor, C_{kk}, is the local average of the squared extension of polymers. The transport equation for C_{ij} is derived from the Fokker–Planck equation (for complete derivation, see Bird et al. 1987):

$$\partial_t C_{ij} + u_k \partial_k C_{ij} = C_{ik}\partial_k u_j + C_{kj}\partial_k u_i - T_{ij} + \frac{1}{ReSc}\partial_k \partial_k C_{ij}\,. \tag{3.}$$

The first two terms on the right-hand side (RHS) of Equation 3 represent the stretching of polymers by the local velocity gradients, the third term is the entropic term or spring force, and the last is the molecular diffusion of C_{ij}, which is a function of the Schmidt number Sc, the ratio of solvent viscosity to diffusivity of polymers in solution. The tensor T_{ij} is the internal stress in Equation 3, as well as the viscoelastic stress in Equation 2,

$$T_{ij} = \frac{1}{Wi}\left[f(C_{kk})C_{ij} - \delta_{ij}\right], \tag{4.}$$

where the Weissenberg number Wi is the relaxation time of the polymer solution normalized by the flow timescale.

The Oldroyd-B model assumes a linear spring connecting the two beads of the dumbbell model, which translates into $f(C_{kk}) = 1$. The simplicity and linearity of the Oldroyd-B model has made it a prime candidate for linear stability analysis, similarly to the upper-convected Maxwell (UCM) model (Section 3.1). The UCM model simply corresponds to the Oldroyd-B model with $\beta = 0$ in Equation 2 (i.e., a polymeric liquid without Newtonian solvent). However, the Oldroyd-B suffers from several limitations. One is the possibility of singular extensional viscosity or stress in extensional flows, owing to the absence of an upper bound on the polymer extensibility. Another is its inability to reproduce the shear thinning behavior observed in most polymer solutions.

A solution to these two limitations is to introduce a nonlinear spring force to limit the dumbbell extension, such as the finitely extensible nonlinear elastic (FENE) spring proposed by Warner (1972). The drawback of the FENE model is that the constitutive equation for the polymer stress is unclosed. A closure can be obtained if a preaveraging, known as the Peterlin approximation, is performed in the calculation of the nonlinear spring force. The resulting FENE-P model is then given by

$$f(C_{kk}) = \frac{1}{1 - C_{kk}/L^2}\,, \tag{5.}$$

Oldroyd-B: Hookean constitutive viscoelastic model

FENE-P: finitely extensible nonlinear elastic-Peterlin constitutive model, derived from a nonlinear internal stress model

UCM: upper-convected Maxwell constitutive model, corresponding to an Oldroyd-B model with $\beta = 0$ (i.e., without solvent)

where L is the finite length of polymer molecules. The FENE-P model is the most popular nonlinear model used in simulations of polymer drag reduction, but the Peterlin approximation reduces its accuracy compared to the FENE model. In particular, FENE-P is not able to show the hysteresis effect that polymers have. It also assumes a homogeneous distribution of single–molecular weight molecules. In real polymer solutions, the distribution of molecular weights is broader, which may produce a spectrum of timescales the FENE-P model cannot reproduce. It should be noted that there are models for multidispersed polymer solutions but they have yet to be tested in EIT. Additionally, it is very difficult to determine the parameters L, Wi, and β to match an actual polymer solution. Although FENE-P has been shown to capture the dynamics of MDR flows and the emergence of EIT in subcritical flows, the reader should bear in mind that exact comparison between simulations and experiments is still a challenge.

2.2. The Diffusion Problem

Polymer diffusion in a typical solvent like water is very small, of the order of 10^{-12} m^2/s (Layec & Layec-Raphalen 1983), corresponding to a Schmidt number of $Sc = 10^6$. This property justifies neglecting the diffusion term in the derivation of constitutive viscoelastic models such as FENE-P (Bird et al. 1987). However, most DNS of Equations 1–3 add a diffusive term (the last term on the RHS of Equation 3) with a Schmidt number much lower than 10^6. Sureshkumar & Beris (1995a) first investigated the impact of the addition of stress diffusion on the numerical stability of a supercritical channel flow ($Re = 5{,}000$). Using a spectral method, the authors found that numerical stability requires a diffusion coefficient $(ReSc)^{-1} = \mathcal{O}(10^{-3})$ or $Sc \sim 0.2$. This study has justified the use of $Sc < 1$ in most subsequent simulations of polymer drag reduction (among the most cited, Sureshkumar et al. 1997, Ptasinski et al. 2003, Stone et al. 2004, Li et al. 2006, Xi & Graham 2010, Thais et al. 2011). The FENE-P model based on $Sc < 1$ captures the drag reduction mechanism of polymer additives (i.e., the damping of near-wall vortices). However, the fundamental modification of the mathematical nature of Equation 3 from hyperbolic ($Sc \gg 1$) to parabolic ($Sc < 1$) has significant consequences on the simulated physics.

Dubief et al. (2005) and Sid et al. (2018) discussed this problem in the framework of small scales of passive scalar transport in turbulent flows developed by Batchelor (1959) and Batchelor et al. (1959) for $Sc < 1$ and $Sc \gg 1$. These two major contributions in turbulence theory define the smallest length scale of passive scalar as a function of the smallest length scale of turbulence, the Kolmogorov scale, $\eta_K = (\nu/\varepsilon^3)^{1/4}$, where ν is the viscosity and ε is the dissipation rate of the turbulent kinetic energy. For $Sc < 1$, the smallest length scale of a passive scalar is the Obukhov–Corrsin length scale, $\eta_{OC} = \eta_K Sc^{-3/4}$, larger than the Kolmogorov length scale by a factor of 1.6 for $Sc = 0.5$ to a factor of 3.3 for $Sc = 0.2$. The Batchelor scale for $Sc \gg 1$, $\eta_B = \eta_K Sc^{-1/2}$, is obviously a factor $\sqrt{Sc}$ smaller than η_K. Dubief et al. (2005) remarked that the stretching and entropic terms in Equation 3 (i.e., the source terms of individual tensor components) do not have any diffusive property and are likely to produce small length scales on the order of the Kolmogorov length scale or smaller. The small-scale dynamics of the exact FENE-P model (with $Sc \to \infty$) is therefore strongly influenced by the convection term $u_k \partial_k C_{ij}$. Since there is no theory available today for active transported properties such as C_{ij}, it is fair to assume that the smallest length scale of this tensor dynamics is between the Kolmogorov and the Batchelor scales, but a key question remains: How far does the dynamic range of scales (i.e., the scales to be resolved to capture the dynamics of polymer flows) extend into the small scales below the Kolmogorov length scale?

2.3. Appropriate Numerical Methods

The previous question cannot be answered with $Sc < 1$. Numerical methods must be adapted to the mathematical nature of the equations, here the hyperbolicity, or stiffness, of Equation 3.

Min et al. (2001) proposed a numerical method typically used in compressible flows for the treatment of the convection term in Equation 3: a higher-order upwind scheme supplemented by a local artificial diffusion triggered by the loss of positiveness of the determinant of C_{ij}, a symmetric tensor. Effectively, such an approach thickens large gradients to adjust to the local mesh resolution. Dubief et al. (2005) modified Min et al.'s algorithm to enforce upper boundedness of the trace of C_{ij}. The algorithm is not unconditionally stable; strong Gibbs oscillations in regions of large gradients can result in a loss of positiveness of one or more diagonal components of the tensor. As expected from stiff problems, convergence is recovered by reducing the time step and increasing the spatial resolution.

Vaithianathan & Collins (2003) proposed a more robust approach with the combination of a higher-order upwind scheme and an eigenvalue decomposition of the conformation tensor. Albeit rigorously robust and respecting the low diffusivity of polymers, the method proved to be costly, and a new iteration (Vaithianathan et al. 2006) resorted to the solution of the C_{ij} transport equation in its naive form, thereby removing the strict enforcement of the upper and lower boundedness of the tensor. A log-conformation approach (Fattal & Kupferman 2005) should also be mentioned for its ability to remain bounded. This method is also quite computationally expensive and has not been applied to the simulation of EIT flows to our knowledge.

Other algorithms that have successfully simulated EIT (e.g., Shekar et al. 2019) use upwinding or limiter schemes for the advection term of the C_{ij}-transport equations. A notable exception is the simulation of Lopez et al. (2019), who used a spectral method with $Sc = 2$ and $L = 30$. The general consensus of available results at the time of writing is that the simulation of large L, Wi, and β values requires the similar compromises used in compressible flows (upwinding or limiters), with the inherent limitations with respect to numerical dispersion and dissipation.

2.4. Computational Domain Limitations

The need for large resolution both in time and space is a limiting factor in the dimensions of the computational domain and its boundary conditions. Since the bulk of EIT research has focused on pipe and channel flows, DNS have mostly used periodic boundary conditions in the streamwise directions. Periodicity is extensively used in inertial turbulent, wall-bounded flows with the constraint that the length of the domain should be long enough for streamwise correlations to reach zero for half the domain's length.

It should not be a surprise that the emerging research in EIT parallels the numerical study of IT in channel flows. The first major contribution was the DNS of Kim et al. (1987) in a doubly periodic channel large enough for correlations to vanish and at low Reynolds number, slightly above the critical Reynolds number. Another key contribution was the demonstration of the existence of minimal flow unit [MFU (Jiménez & Moin 1991)], which isolated the set of coherent structures responsible for the self-sustaining process of turbulence. As an intermediate state, Jiménez (1994) and Orlandi & Jiménez (1994) studied a 2D vortex to gain further understanding in the generation of friction and control of wall-bounded flows. From these works emerged a clearer picture of the self-sustaining mechanism of wall turbulence (Waleffe 1997, Jiménez & Pinelli 1999) and the concept of exact coherent structures (ECS) in wall-bounded flows (Waleffe 2001). Later, as computing power increased and algorithms improved, higher–Reynolds number simulations in very large domains enabled the investigation of very large-scale dynamics (Jiménez et al. 2001).

In the timeline of wall turbulence research, at the time of publication, EIT has reached the level of Jiménez & Moin's MFU and ECS. The simulations are still limited to small 2D and 3D domains, inhibiting our ability to study the effects of very large scales on EIT and adding uncertainties when comparing with experiments. For example, the relaminarization observed experimentally by

Choueiri et al. (2018) may be observed in 2D channel flow for a given length. However, increasing this length for the same polymer parameters may drive the flow to a more chaotic state (Dubief et al. 2022). Whereas there is value in manipulating or cutting-off scales to better understand the dynamics, caution should be exercised when comparing simulations to experiments that are spatially developing over much greater lengths than what is computationally affordable in 2023. The investigation of very large scales will most likely require advances in algorithms and hardware to overcome the requirements for spatial and temporal resolutions much finer than those for inertial turbulence at comparable Reynolds numbers.

Future research should advance our understanding of 2D and 3D flows. Whereas the latter is obviously more expensive and the former contains the key elements of the self-sustaining mechanisms of EIT (Sid et al. 2018), experiments are ultimately 3D. Two-dimensional simulations must be viewed as numerical experiments, much like the MFU of Jiménez & Moin. For 3D simulations, it should not be assumed that EIT's dynamics can be fully contained in domains that are deemed adequate for IT. Rather, the community should invest time into a careful investigation of the influence of boundary conditions and domain sizes on the dynamics of EIT.

2.5. Lessons and Perspective

Although early turbulence was the first sign of EIT, numerical simulations shed crucial light on its possible structure (which is discussed below) and domain of existence, which extends well into the polymer drag reduction regime. In fact, the numerical methods that successfully simulate EIT highlight key elements of its physics. The stiffness of Equation 3 requires higher resolution than for Newtonian flows and much smaller time steps. Low–Schmidt number diffusion effectively filters out EIT, as shown by Sid et al. (2018), whose simulations ($Sc = \infty$, local artificial diffusion) establish clear EIT dynamics for the same parameters for which Xi & Graham (2010) simulated a laminar flow ($Sc = 0.5$). Hyperbolicity is not only critical to the existence of EIT but also necessary for its sustainability.

Upwind schemes and centered finite difference/volume schemes carry inherent dispersion, which can result in a spurious accumulation of energy at small scales, even with the high-wavenumber numerical dissipation of the upwind schemes. Despite extensive resolution studies (Sid et al. 2018, Dubief et al. 2022), this numerical dispersion has cast uncertainty on simulated EIT since its discovery. However, if the problem is simply stiff, it ought to be solvable with nondissipative, nondispersive numerical methods (i.e., spectral methods), provided that the resolution is high enough and the time step is low enough. Berti et al. (2008) showed this proposition to be true in the simulation of elastic turbulence in low-*Re* Kolmogorov flow.

The importance of small-scale resolution is undeniable; however, Batchelor et al.'s (1959) theory for $Sc \gg 1$ passive scalars must be considered as a guideline. Dominant energy transfers between turbulent kinetic energy and turbulent elastic energy occur around Kolmogorov scales. Spectra of C_{ij} or elastic energy have not shown clear k^{-1} energy decay beyond the Kolmogorov wavenumber. However, the study of energy spectra as a function of Schmidt number (Sid et al. 2018) shows a clear reduction of energy at all scales for $Sc < 100$ at a Reynolds number in the critical to supercritical range. The prediction of the smallest relevant dynamic scale for the polymer field remains an open question.

A different development is the recent efforts to simulate EIT in wall-bounded flows with spectral methods by the present authors and others at large Sc, which may allow for the rigorous elimination of numerical dispersion and dissipation for spatial derivatives of current algorithms. It is hoped and anticipated that this new development in the numerical simulation of EIT will lead to a thorough assessment of the effect of Schmidt number on the dynamics of EIT and to

the definition of criteria for spatial and temporal resolutions as a function of flow and polymer parameters.

However, it is critical to stress that the simulation of EIT using Eulerian constitutive equations such as Equations 1–4 with current algorithms is a long and frustrating endeavor of high-resolution simulations that must be run for very large flow times with time steps much smaller than those of comparable Newtonian simulations. Any shortcut has so far resulted in a loss of critical dynamics. Future algorithms should focus on resolving the stiffness of Equation 3 with the highest fidelity at the lowest possible cost. It is hoped that the emergence of hybrid computing platforms (CPU + GPU) could make these simulations more tractable, as they have for other stiff problems like molecular dynamics (Páll et al. 2020).

3. ONSET OF ELASTO-INERTIAL TURBULENCE

Early studies failed to detect a linear instability in (non-shear-thinning) viscoelastic pipe flow and, at low Reynolds number, channel flow. However, these studies only investigated low Weissenberg numbers. In the absence of inertia, linear instability was only found for flows with curved streamlines (Larson et al. 1990, McKinley et al. 1991, Shaqfeh 1996). As a result, parallel shear flows of viscoelastic fluids were for a long time believed to be linearly stable in the low-*Re* limit (Larson 1992, Wilson et al. 1999).

At larger Reynolds numbers, the linear stability of Newtonian pipe and Couette flows (Schmid & Henningson 2000) has been widely assumed to also apply to the viscoelastic case. On the other hand, earlier studies of plane Poiseuille flow of a UCM fluid have found several unstable modes (Porteous & Denn 1972), in addition to the elastically modified Tollmien–Schlichting (TS) mode that is known to become unstable in the Newtonian limit at $Re_c = 5{,}772$ (Schmid & Henningson 2000). However, these modes are strongly stabilized by the solvent viscosity (Sureshkumar & Beris 1995b) and thereby become irrelevant in the dilute limit. Moreover, the elastically modified TS mode shows a nonmonotonic behavior with increasing elasticity number E (Sureshkumar & Beris 1995b, Zhang et al. 2013), the ratio of the Weissenberg number Wi to the Reynolds number Re,

$$E = \frac{Wi}{Re}. \qquad 6.$$

Inspired by the discovery of ET in inertialess flows with curved streamlines (Groisman & Steinberg 2000), several studies investigated the possibility of a purely elastic nonlinear instability leading to a state analogous to elastic turbulence in planar shear flows (Morozov & Saarloos 2005, 2007, 2019). These authors argued that perturbations inducing sufficient flow curvature could possibly trigger a nonlinear instability akin to the purely elastic instability in Taylor–Couette flows. Initial perturbations in the form of blowing and suction at the wall are, for instance, frequently used in numerical simulations to initiate the chaotic dynamics of EIT (Dubief et al. 2013).

On the other hand, several experimental observations hinted at a possible supercritical viscoelastic instability (Little et al. 1975, Samanta et al. 2013, Choueiri et al. 2018, Chandra et al. 2020, Choueiri et al. 2021). In particular, the smooth and continuous transition from the laminar regime to MDR, the absence of hysteresis when increasing or decreasing the fluid elasticity, the invariance of the critical Reynolds number for externally perturbed and unperturbed transition at sufficiently large concentration, and the disappearance of localized puffs (a signature of the nonlinear subcritical route in the Newtonian case) were all indications of a possible linear instability of the viscoelastic pipe flow to which Forame et al. (1972), Graham (2014), or Wen et al. (2017) had previously alluded. The existence of such linear instability at large Weissenberg number has been recently confirmed by (Garg et al. 2018), as discussed below.

One of the main difficulties in obtaining a clear picture on the scenarios of transition to EIT is the high dimensionality of the parameter space (Reynolds number, Weissenberg or elasticity number, polymer-solvent concentration, etc.). On the other hand, this also offers several pathways to EIT that do not rely on the modification of Newtonian ECS, as previously postulated (Zhu & Xi 2021).

3.1. Recent Linear Stability Results for Viscoelastic Pipe and Channel Flows

Motivated by the abovementioned experimental hints at a possible linear instability, Garg et al. (2018) revisited the stability of the viscoelastic pipe flow. Using the Oldroyd-B model, they demonstrated that for large Weissenberg numbers the viscoelastic pipe flow can be linearly unstable to axisymmetric disturbances down to a critical Reynolds number $Re_c \approx 63$, much lower than the Newtonian transition threshold. Newtonian turbulence is only sustained for $Re > 2{,}040$ and turns transient below this critical point (Avila et al. 2011, Mukund & Hof 2018).

The viscoelastic linear instability has been further detailed and analyzed by Chaudhary et al. (2021). The unstable mode is found to propagate at a speed close to the base state maximum velocity and has thus been called a center mode, although its disturbance field is spread across the entire pipe cross section. A more significant localization of the velocity eigenfunctions toward the pipe center is only observed at larger Reynolds numbers. The absence of instability in the Newtonian ($\beta = 1$ or $Wi = 0$) and UCM limits suggests that inertia, viscous solvent stress, and elastic polymer stress are essential for this center mode instability. In the asymptotic limit of dilute polymer solutions, $(1 - \beta) \ll 1$ and $E(1 - \beta) \ll 1$, the critical Reynolds number scales as $Re_c \propto [E(1 - \beta)]^{-3/2}$ (i.e., $Wi_c \propto Re_c^{1/3}$). In other words, the instability survives given $E \propto (1 - \beta)^{-1}$, so that the polymer stress of the disturbance remains of order unity. Additionally, there is a maximum elasticity number E_c (i.e., $Wi_c \propto Re_c$) above which the instability does not exist for any Re, as illustrated by the neutral curves in **Figure 4*a***. To take into account the effect of shear thinning (FENE-P model), Chaudhary et al. (2021) also suggested that the above $-3/2$ exponent

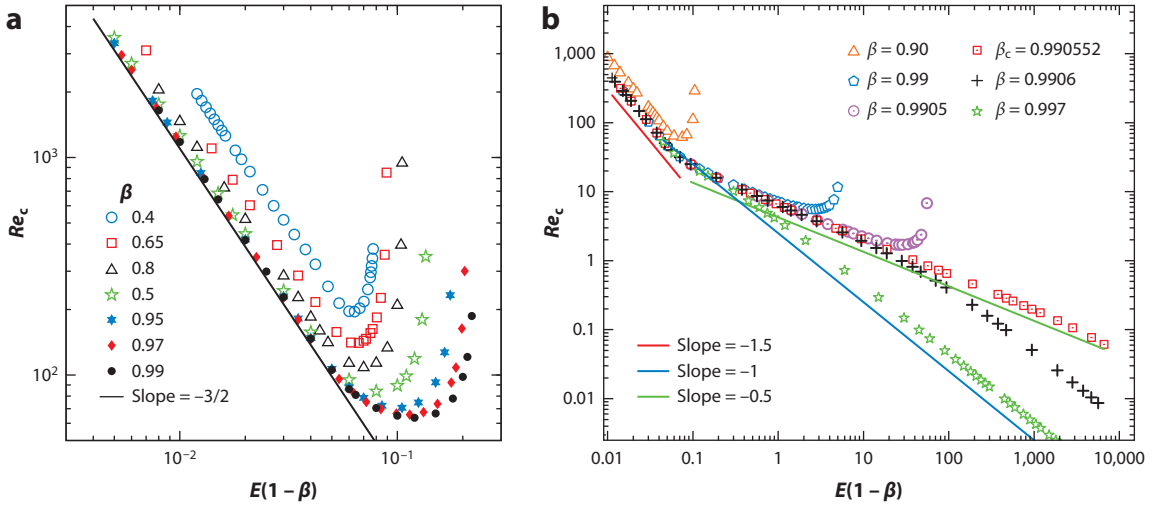

Figure 4

Critical Reynolds number Re_c as a function of the elasticity number E (see Equation 6) weighted by $(1 - \beta)$, with β the ratio of solvent viscosity to the viscosity of the zero–shear polymer solution, for different values of β in the case of the (*a*) pipe and (*b*) channel flow of an Oldroyd-B fluid. Panels adapted with permission from (*a*) Chaudhary et al. (2021), copyright 2021 the authors, and (*b*) Khalid et al. (2021b), copyright 2021 American Physical Society.

be replaced by $-5/8$. The parameter space was then extended by Dong & Zhang (2022), who carried out an asymptotic analysis through singular perturbations.

In light of the similarities between Newtonian pipe and channel flows, it comes as no surprise that, in addition to the elastically modified Newtonian TS mode, a very similar center mode instability also exists in the plane Poiseuille flow of an Oldroyd-B fluid at sufficiently high elasticity (Khalid et al. 2021a). The same asymptotic scaling of the critical Reynolds number Re_c as that in the pipe flow for dilute solutions indicates a possible universal linear mechanism underlying the onset of EIT in both pipe and channel configurations. Nonetheless, the center mode instability ceases to exist in channel flow for $\beta < 0.5$. On the other hand, unlike initially thought (Ho & Denn 1977), it continues to exist down to $Re = 0$ in ultradilute solutions ($\beta > 0.9905$) at very high Weissenberg number (Khalid et al. 2021b), as illustrated by the corresponding neutral curves in **Figure 4*b***. These results suggest the existence of a continuous pathway between ET and EIT, directly connected to the laminar state. The inclusion of finite extensibility (FENE-P model) seems to move the neutral curve closer to the inertialess limit at fixed β and toward lower, and more realistic, critical Weissenberg numbers in the dilute limit (Page et al. 2020, Zhang 2021). In the absence of solvent (UCM, $\beta = 0$) Chaudhary et al. (2019) found several symmetric and antisymmetric unstable wall modes. The addition of solvent (small but finite β), however, leads to a strong stabilization of these modes, in stark contrast to the destabilizing effect of solvent viscosity on the center mode.

It should finally be mentioned that most of these recent linear stability studies rely on a new geometric decomposition of the conformation tensor and the associated scalar measures of the polymer perturbations introduced by Hameduddin et al. (2018, 2019). This new formalism ensures that the mean and perturbation tensor fields remain positive definite. It thus provides a rigorous mathematical basis for analysis and allows a clear physical interpretation compared to the Euclidean geometry assumed by the classical decomposition. This framework is useful not only in linear and nonlinear stability theory but also more generally when analyzing the conformation tensor.

3.2. Nonmodal Amplification

Modal stability analysis only focuses on the asymptotic long-time growth rate of perturbations. Because the operators of the linearized equations are not self-adjoint (nonnormal), the linear eigenmodes are typically nonorthogonal, which can lead to an initial algebraic transient growth before the long-term exponential decay (Schmid 2007). Transient amplification can thus produce perturbations that become larger than the nonlinear instability threshold of a subcritical bifurcation.

Whereas the potential importance of transient growth has already been recognized (e.g., Doering et al. 2006), much work has recently been dedicated to investigating the nonmodal amplification of infinitesimal perturbations, including that of Jovanović and colleagues (Hoda et al. 2008, 2009; Jovanović & Kumar 2009, 2010, 2011; Hariharan et al. 2018), Zaki and colleagues (Zhang et al. 2013; Agarwal et al. 2014; Page & Zaki 2014, 2015), Graham and colleagues (Shekar et al. 2019, 2020), and Zhang (2021). A good overview of the topic is given by Sánchez et al. (2022).

While nonmodal analysis cannot prove the existence of a subcritical instability, it offers an amplification mechanism that may lead to a self-sustained nonlinear state.

3.3. Subcritical Transition

Although the linear instability of viscoelastic pipe and channel flows suggests a possible route to EIT through a supercritical transition, turbulence was detected in experiments of viscoelastic pipe flow (including older studies on structural/early turbulence) down to far lower Reynolds numbers ($Re \approx 1$), and in simulations at lower Weissenberg numbers, than the instability threshold in linear

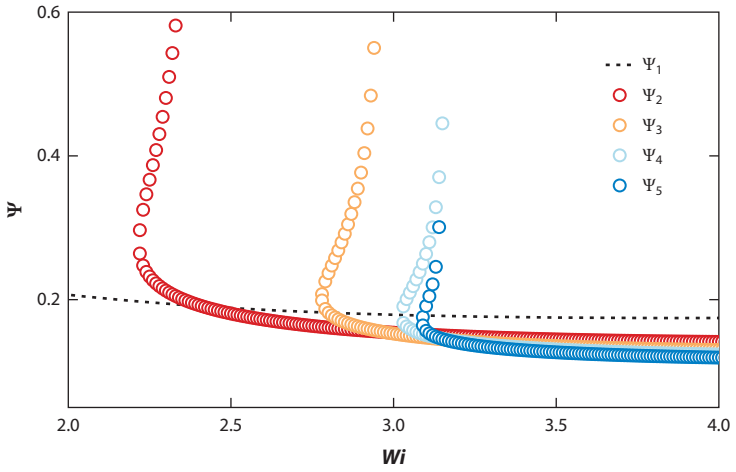

Figure 5

Nonlinear perturbative expansion: convergence of the amplitudes Ψ_m of traveling wave solutions as functions of the Weissenberg number *Wi* for the case of plane Poiseuille flow of an Oldroyd-B fluid with concentration parameter $\beta = 0.05$. The lower branch defines the perturbation amplitude required to destabilize the flow. Figure adapted from Morozov & Saarloos (2019) (CC BY 4.0).

analysis. There is consequently a large part of the parameter space outside the linearly unstable regions in which EIT has been observed, highlighting the existence of bifurcated solutions beyond the parameter domain of linear instability. This implies that the viscoelastic flow is possibly nonlinearly unstable (i.e., unstable to sufficiently large-amplitude disturbances). Moreover, akin to the Poiseuille flow whose linear instability is in practice quite irrelevant, linear instability does not preclude a nonlinear subcritical transition. Such a subcritical scenario has been proposed as most likely (Morozov & Saarloos 2007), and experimental evidence has corroborated this in the low–Reynolds number limit (Pan et al. 2013, Qin & Arratia 2017).

Using nonlinear amplitude expansion about the Gorodtsov & Leonov (1967) modes, Meulenbroek et al. (2004) and Morozov & Saarloos (2005) obtained clear evidence for a subcritical transition in inertialess plane Poiseuille and Couette flows of a UCM fluid at a Weissenberg number somewhat larger than unity. Their results have been recently extended by Morozov & Saarloos (2019) for an Oldroyd-B fluid in the low-β limit, showing that, even if the laminar flow has straight streamlines and is linearly stable in the parameter range considered, a slowly decaying perturbation with curvature in its streamlines can drive an instability (see **Figure 5**). Similarly to the Newtonian case, the resulting nonlinear structures are traveling wave solutions characterized by the presence of vortices, streaks, and high polymer stress in the near-wall region.

Our current understanding of Newtonian transition relies on a dynamical system interpretation, in which the transitional flow is seen as a wandering trajectory in phase space between different nontrivial 3D solutions of the Navier–Stokes equations, the so-called ECS solutions (Kerswell 2005, Eckhardt et al. 2007, Graham & Floryan 2021). A similar interpretation for the viscoelastic case could also be envisioned, where EIT would be built around the coexistence of many (unstable) simple invariant solutions populating the phase space but that rely on elasticity to exist (Morozov & Saarloos 2019). This scenario has gained support with the recent discovery of the first coherent structure in 2D EIT by Dubief et al. (2022). This stable attractor in 2D takes the particularly simple form of a traveling wave in which sheets of large polymer stress originating near the walls bend to meet at the channel center to form a symmetric arrowhead structure (see the detailed discussion in Section 4).

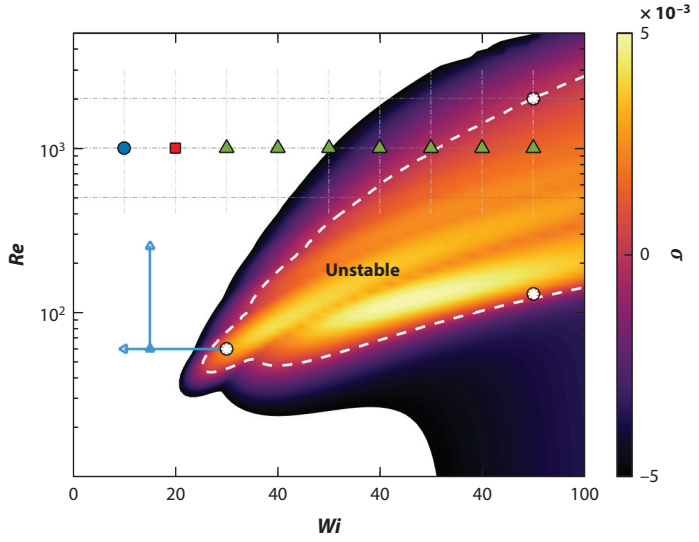

Figure 6

Contours in the Weissenberg number (*Wi*)–Reynolds number (*Re*) stability diagram of the linear growth rate σ of perturbations for most unstable symmetric instability waves in a 2D channel flow of a FENE-P (finitely extensible nonlinear elastic-Peterlin) fluid ($L = 500$) for streamwise wavenumbers $k \in \mathbb{N}$. The dashed white line indicates marginal stability, $\sigma = 0$. The overlayed grid and symbols identify direct numerical simulations in a box of length $l_x = 2\pi$: laminar (*blue circle*), elasto-inertial turbulence (*red square*), and arrowhead structure (*green triangles*). The blue lines identify the arclength continuation of the nonlinear traveling wave born in this instability (at $k = 2$). The white circles refer to visualization of the instability waves in the physical space, available in figure 2*b* of Page et al. (2020). Figure adapted from Page et al. (2020) with permission; copyright 2020 American Physical Society.

Despite significant differences between the arrowhead structure and the linearly unstable center mode, Page et al. (2020) recently established a clear link between the two by tracking the traveling wave issued from the saturated center mode linear instability in Weissenberg and Reynolds number (see **Figure 6**). Their analysis demonstrates the subcriticality of the bifurcation at this point. The upper-branch solution corresponds to the arrowhead solution of Dubief et al. (2022), while the much weaker lower-branch states resemble more closely the center mode eigenfunction of Garg et al. (2018). It is interesting to note that the threshold of the perturbation amplitude for nonlinear instability is low, even at much lower *Wi* than its value at the bifurcation, implying that for practical purposes the instability might appear supercritical. The weakly nonlinear analysis of Buza et al. (2022) also shows that the subcriticality of the center mode linear instability is generic across the neutral curve (also in β at $Re = 0$) with supercritical bifurcation only in the low-*Re*, high-*Wi* region of the parameter space. Destabilization is found to be elastically driven rather than inertia driven, as the polymer work and not the shear energizes the instability. On the other hand, at higher polymer concentration (low β), the unstable region becomes smaller and the transition is mostly supercritical (Wan et al. 2021, Buza et al. 2022).

Another subcritical route, based on viscoelastic wall modes strongly localized at the critical layer, has been proposed by Shekar et al. (2019) in plane Poiseuille flow for moderate Weissenberg numbers. This family of attractors, which are nonlinearly self-sustained, resembles the stable Newtonian TS mode and is connected to 2D EIT through an unstable branch (Shekar et al. 2020). At moderate Reynolds number, the Newtonian and viscoelastic TS attractors are disconnected in phase space. However, Shekar et al. (2021) have shown that, at $Re = 10{,}000$, the unstable

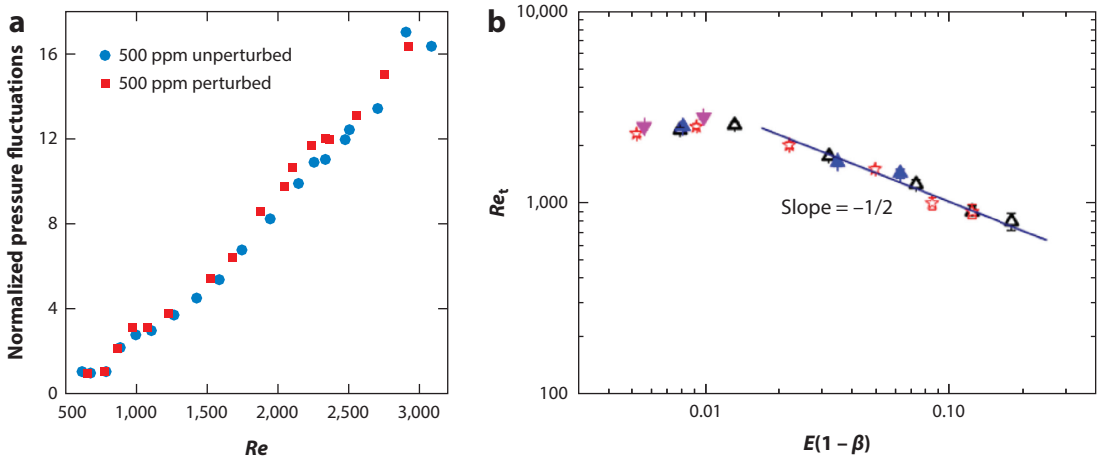

Figure 7

(*a*) Continuous increase of pressure fluctuations with Reynolds number *Re* at the onset of elasto-inertial turbulence. Panel adapted from Samanta et al. (2013) with permission; copyright 2013 the authors. The threshold is found to be independent of external perturbations and, hence, no hysteresis could be detected. (*b*) Scaling of the transition threshold Reynolds number Re_t with the elasticity number *E* weighted by $(1 - \beta)$, where β is the ratio of the solvent viscosity to the zero-shear viscosity of the polymer solution. Panel adapted from Chandra et al. (2018) with permission; copyright 2018 Cambridge University Press.

Newtonian TS attractor evolves continuously into EIT upon increasing the Weissenberg number. The importance of wall modes and critical layers has also been confirmed through resolvent analysis in channel flow (Shekar et al. 2019) and pipe flow (Zhang 2021).

3.4. Experimental Observations

In experiments, EIT appears to arise continuously with increasing shear rate, as shown in **Figure 7**. Hence, unlike for the Newtonian turbulence transition, no hysteresis is detectable at the onset of EIT. In these measurements the onset of EIT has been detected by monitoring pressure fluctuations. While in experiments pressure fluctuations are also nonzero in laminar flow, this background noise level is constant and independent of *Re*. The transition is then characterized by a continuous increase in fluctuations.

The possibility of a supercritical transition seems to be corroborated by the pipe experiment of Chandra et al. (2020), who observed a departure from the laminar friction factor *f* with the transition Reynolds number Re_t in the form $(f/f_{lam} - 1) \propto (\mathrm{Re}/\mathrm{Re}_t - 1)^{1/2}$. The ET experiment of Jha & Steinberg (2021) would also suggest a linear instability at high *Wi*. Reasonable agreement is also found between linear stability predictions and the experiment of Srinivas & Kumaran (2017) in microchannels.

Despite the apparent continuous nonhysteretic scaling, the distinction of a supercritical from a subcritical transition is not straightforward in this case. Looking at flow structures close to onset, Choueiri et al. (2021) detected a chevron-type flow pattern, illustrated in **Figure 8**, which is in good qualitative agreement with the unstable mode predicted by Garg et al. (2018). However, even close to onset the flow in experiments remained unsteady and 3D. Hence, the flow never fully settled to the mode predicted by linear theory. Moreover, the same authors also observed the corresponding fluctuating chevron structure down to *Re* as low as 5 (see the top panel of figure 1*B* of Choueiri et al. 2021), while stability analysis only predicts a linear instability for $Re \gtrsim 60$. Although quantitative differences between experiments and the stability of an Oldroyd-B

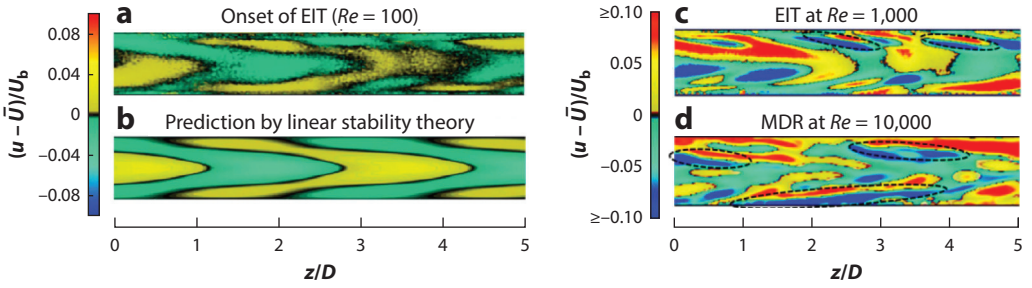

Figure 8

Structure of elasto-inertial turbulence (EIT). Choueiri et al. (2021) captured the structure of EIT in experiments using particle image velocimetry. (*a*) The flow field close to the onset of EIT (Reynolds number $Re = 100$, Weissenberg number $Wi = 304$, concentration parameter $\beta = 0.5$): Plotted is the streamwise velocity component u minus the average profile $\bar{U}$ and normalized by the bulk flow speed U_b. The overall structure is that of a center mode, which is in qualitative agreement with the linear stability prediction (Garg et al. 2018) (*b*). (*c*) Further above the onset of instability, however, EIT is largely composed of near-wall streak-like structures at $Re = 1{,}000$ (*dashed ovals*). Qualitatively, the flow structure remains unchanged with increasing Re and persists in the maximum drag reduction (MDR) limit here shown for $Re = 10{,}000$ (*d*). Figure adapted from Choueiri et al. (2021) with permission; copyright the authors.

fluid may be expected, the Reynolds number threshold in experiments is more than an order of magnitude lower. This, just like the unsteady nature of the flow patterns, points to a subcritical scenario. In this context it should be noted that, if transition thresholds are finite but smaller than or equal to the noise level in experiments, a subcritical transition cannot be readily distinguished from a supercritical one. Recent theoretical studies (Wan et al. 2021, Buza et al. 2022) indeed propose low-amplitude thresholds in the subcritical regime for EIT.

Furthermore, above the onset of EIT (e.g., **Figure 8*c***) Choueiri et al. (2021) reported a structural change from the chevron center mode to a wall mode. At this higher Reynolds number EIT is dominated by near-wall inclined shear layers and streak pairs. Interestingly this structural composition of EIT is equally found at ten times larger Re in the MDR limit (**Figure 8*d***).

3.5. Discussion and Perspective

Clearly, the high dimensionality of the parameter space offers several possible routes to EIT, as tentatively summarized in **Figure 9**. At high elasticity, in both pipe and channel flows, the unstable center mode allows for a supercritical path to transition, but the instability in dilute solutions is likely to be subcritical in a large part of the parameter space. Additionally, in channel flow, the center mode instability extends down to $Re = 0$ for ultradilute solutions, and an elastically modified TS mode provides an additional nonlinear subcritical route at moderate Reynolds and Weissenberg numbers. Because it is believed that even relatively weak viscoelasticity tends to suppress the Newtonian ECS (Li & Graham 2007), subcritical transition to EIT is likely based on new elasto-inertial coherent states, such as the arrowhead attractor (Dubief et al. 2022) or the viscoelastic nonlinear TS attractor (Shekar et al. 2020), which are sampled by an EIT trajectory akin to the Newtonian case.

This picture is certainly incomplete and numerous questions remain open. The supercritical transition to EIT has yet to be reproduced in numerical simulations, and the subsequent steps following the initial linear instability (nonlinear saturation, secondary instabilities) need to be elucidated. One can also wonder what happens at even higher Weissenberg number for not too dilute solutions—i.e., in regions above the upper branch of the neutral curve in **Figure 9** where the center mode is again stable and the instability likely supercritical. Would the flow be laminar? Do other instabilities exist?

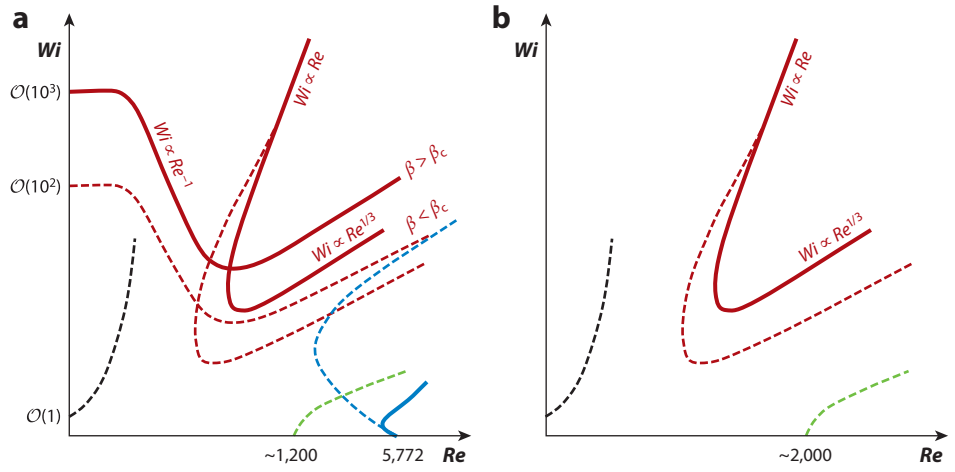

Figure 9

Possible stability map in the Reynolds number (*Re*)–Weissenberg number (*Wi*) plane of (*a*) channel and (*b*) pipe flow of an Oldroyd-B fluid, showing the neutral curve of linear instability (*thick lines*) and the subcritical boundary (*dashed lines*). Center mode instability (*red*) continues down to $Re = 0$ in channel flow for $\beta > \beta_c$. The Newtonian subcritical scenario based on elastically damped exact coherent structures is indicated by the dashed green lines, the viscoelastic nonlinear Tollmien–Schlichting mode is indicated by blue lines, and the subcritical transition leading to elastic turbulence in the inertialess limit is indicated by the dotted black lines. Each curve additionally depends on the concentration parameter β. Figure adapted from Sánchez et al. (2022) with permission; copyright 2022 Elsevier.

On the other hand, the extent of the subcritical regions is widely unknown; saddle nodes can only be located through continuation, and the parameter space is vast. In that respect, the relevance of the elastically modified TS route for pipe flow is still unclear. More generally, the existence of other elasto-inertial attractors and corresponding bifurcations need to be further analyzed.

Khalid et al. (2021a) have shown that the least stable modes in channel flow change from TS to modes in the continuous spectrum (CS) to the center mode when the elasticity is increased. The possible role of CS modes in a subcritical route has not yet been studied. On the other hand, in the inertialess limit the center mode offers an alternative to the previously prevalent view of a bifurcation from infinity. All these modes could thus represent good starting points for a nonlinear expansion, extending thereby the nonlinear analysis of Morozov & Saarloos (2019) to the inertial range and higher Weissenberg numbers.

The center mode has demonstrated a possible continuous path from ET to EIT in channel flow, and the analysis of Buza et al. (2022) suggests that the center mode is elastically driven and not inertia driven. However, this link has not yet been shown in pipe flow. More fundamentally, the connection between EIT and ET, on one side, and between EIT and IT, on the other, needs to be further analyzed. The integration of nonmodal mechanisms into this overall picture would also be very beneficial.

Finally, it should be emphasized that these results have been predominantly obtained using the Oldroyd-B and, to some extent, FENE-P models (Bird et al. 1987). Although these constitutive models incorporate many features of dilute polymer solutions, such as a nonzero first normal stress difference (anisotropy), memory (relaxation), elasticity, and, for the FENE-P model, shear-thinning, they are based on some strong simplifications. This approximate representation of real viscoelastic fluids renders a quantitative comparison with experiments very challenging, especially with regard to the difficult task of determining the numerical parameters (*Wi*, β, *L*, etc.) of the

physical models. Additionally, other instabilities or relevant modes could exist beyond those found with these aforementioned models. For instance, Couette flow is linearly unstable with the nonlinear Phan-Thien–Tanner model (Grillet et al. 2002), while it has otherwise always been found to be linearly stable.

N_1: first normal stress difference

In summary, stability analysis and numerical simulations have greatly helped rationalize experimental observations. Nonetheless, the direct link between them is yet to be fully established. This will require the ability to quantitatively predict the instability thresholds and direct experimental observation of the flow structures predicted by the theory.

4. THE STRUCTURE OF ELASTO-INERTIAL TURBULENCE

4.1. The Different Regimes of Stress Fields in 2D Flows

A significant simplification in the exploration of EIT came from the demonstration that the essential dynamical structures exist in 2D flows (Sid et al. 2018). The dynamical importance of small and large scales renders 3D simulations expensive in both temporal and spatial resolution. Dubief et al. (2022) conducted a comprehensive study of 2D periodic channel flows using the FENE-P model (Equations 1–3) over a large range of Reynolds numbers, polymer parameters (L, Wi, and β), and computational domain lengths. These authors identified the existence of at least four regimes of EIT, including a first ECS.

The structure of polymer stress may be investigated through various quantities that give the same depiction of the dynamics, namely, the trace of C_{ij}, the trace of T_{ij}, the elastic energy $e_p = -L^2/(2ReWi)\ln(1 - C_{kk}/L^2)$, or the first normal stress difference $N_1 = T_\parallel - T_\perp$, where $T_\parallel$ and $T_\perp$ are the diagonal components of the polymer stress tensor aligned and perpendicular to the principal direction of stretch, respectively. The latter quantity is directly related to the extensional viscosity (Bird et al. 1987) as well as, with the second normal stress difference, to the well-known Weissenberg effect in polymer flows, or rod climbing phenomenon, where the first normal stress difference acts like a hoop stress (Barnes et al. 1989).

4.1.1. Chaotic regimes (CR). **Figure 10*a*,*b*** depicts the most CR observed in 2D channel flows. The observed structures of N_1 and pressure contours are very similar to those observed in planes aligned with the streamwise and wall-normal directions in 3D simulations (Dubief et al. 2013, Samanta et al. 2013, Terrapon et al. 2015, Sid et al. 2018).

In the first EIT regime, the CR, regions of large N_1 are organized in thin sheets tilted upward and downstream. A typical sheet displays some undulations, which appear to be connected to low and high cylindrical pressure regions, highlighted at their center in **Figure 10*a*,*b***. These undulations are reminiscent of the undulations of streamlines observed in the original simulation of EIT (Dubief et al. 2010). The fluid gap between two adjacent sheets is therefore subjected to normal stress, whose variations are governed by the relative undulations of the sheets.

The next regime found by increasing elasticity of the solution is the chaotic arrowhead regime (CAR) (**Figure 10*c*,*d***). This regime retains the chaotic sheet structure of CR, but a few sets of two sheets (here, one set) located on either side of the centerline connect to form an arrowhead-looking structure at the center of the channel. This structure is chaotic with very poor symmetry, yet persistent over very long flow times.

4.1.2. Intermittent and steady regimes. Further increase in elasticity leads to the intermittent arrowhead (IAR) and eventually steady arrowhead regime (SAR), depicted in **Figure 10*e*–*h***, respectively. SAR is a fully steady state regime with perfect symmetry about the centerline. IAR is a regime that oscillates between CAR and SAR over timescales much greater than the timescales

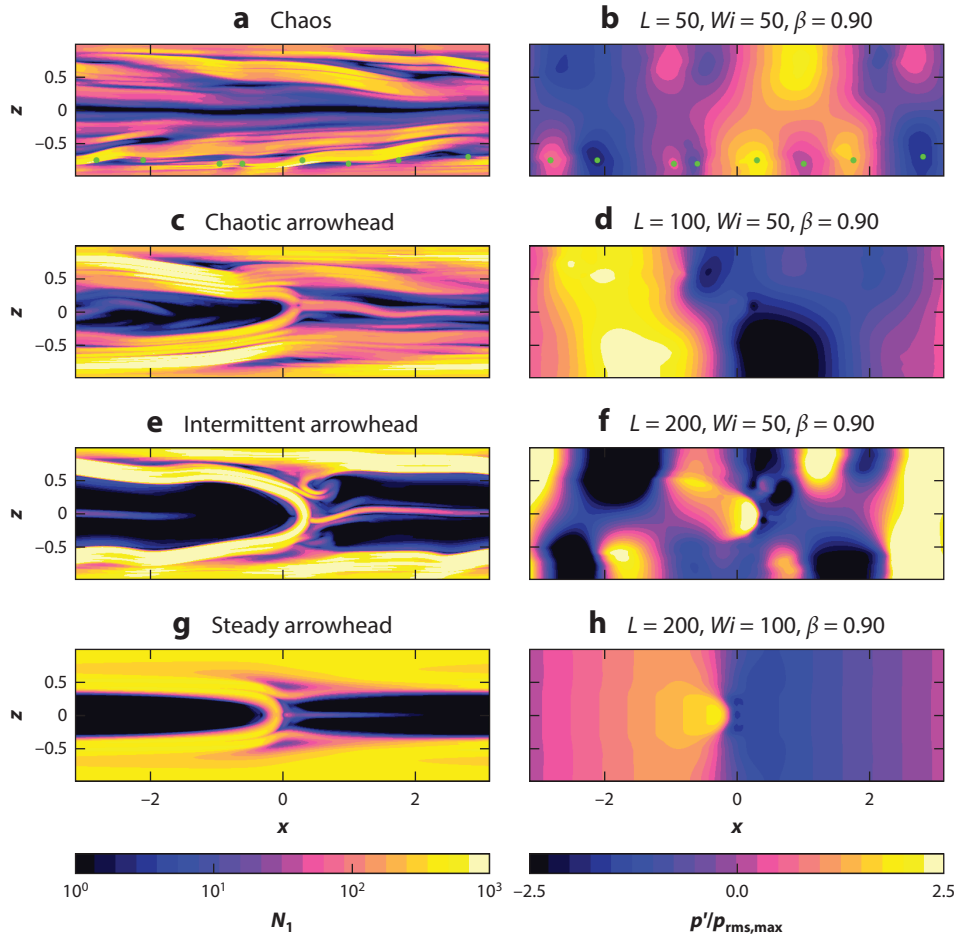

Figure 10

The four regimes of elasto-inertial turbulence identified by Dubief et al. (2022). Snapshots of the first normal stress difference N_1 (*a*,*c*,*e*,*g*) and pressure $p'/p_{\mathrm{rms,\,max}}$ (*b*,*d*,*f*,*h*) contours for different polymer parameters, highlighted in the figure for each regime: chaos (*a*,*b*), chaotic arrowhead (*c*,*d*), intermittent arrowhead (*e*,*f*), and steady arrowhead (*g*,*h*). These regimes are shown here for a bulk Reynolds number of $Re_b = 1{,}000$ in a domain of dimensions $2\pi h \times 2h$. Figure adapted from Dubief et al. (2022) with permission; copyright 2022 American Physical Society.

of chaos in CR and CAR. A distinct feature of the arrowhead structure is its pressure signature, where a high-pressure region is nested under the tip of the arrowhead, or junction of the upper and lower sheets of significant N_1. In SAR, a steep pressure gradient, akin to a shockwave, can be observed at the tip of the arrowhead.

The existence of arrowheads and their regime are highly dependent on the length of the domain, Reynolds number, and the three parameters of the FENE-P model. To summarize, in the first study of this vast parameter space (Dubief et al. 2022), the stability of the arrowhead increases with increasing polymer maximum extension L and Weissenberg number Wi, independently or collectively. The β parameter, which controls the contribution to the solvent viscosity, enhances stability as it decreases, but promotes the emergence of chaos as it approaches unity, suggesting

a stabilizing mechanism associated with decreasing β. For $\beta \to 1$, larger L or Wi are required to return to SAR. A SAR regime in a given domain length eventually becomes unstable as the streamwise length is increased, pointing out a significant role of large scales in the dynamics of EIT. Stability can be recovered by increasing L or Wi at constant β, or by reducing β.

4.2. 3D Structure

Owing to the cost of simulating EIT, the parameter space so far explored in 3D is much more limited than in 2D. The first evidence of EIT was found in a numerical experiment designed to elucidate the phenomenon of early turbulence discussed in Section 1.2. Dubief et al. (2010) conducted a bypass transition in a 3D periodic channel flow. As explained in **Figure 11**, the simulation was designed to trigger transition via a receptivity-like mechanism. Receptivity (Goldstein & Hultgren 1989) defines the energy of pertubations in free-stream that penetrate a boundary layer and trigger instabilities. Here the perturbations are introduced away from the wall and yet

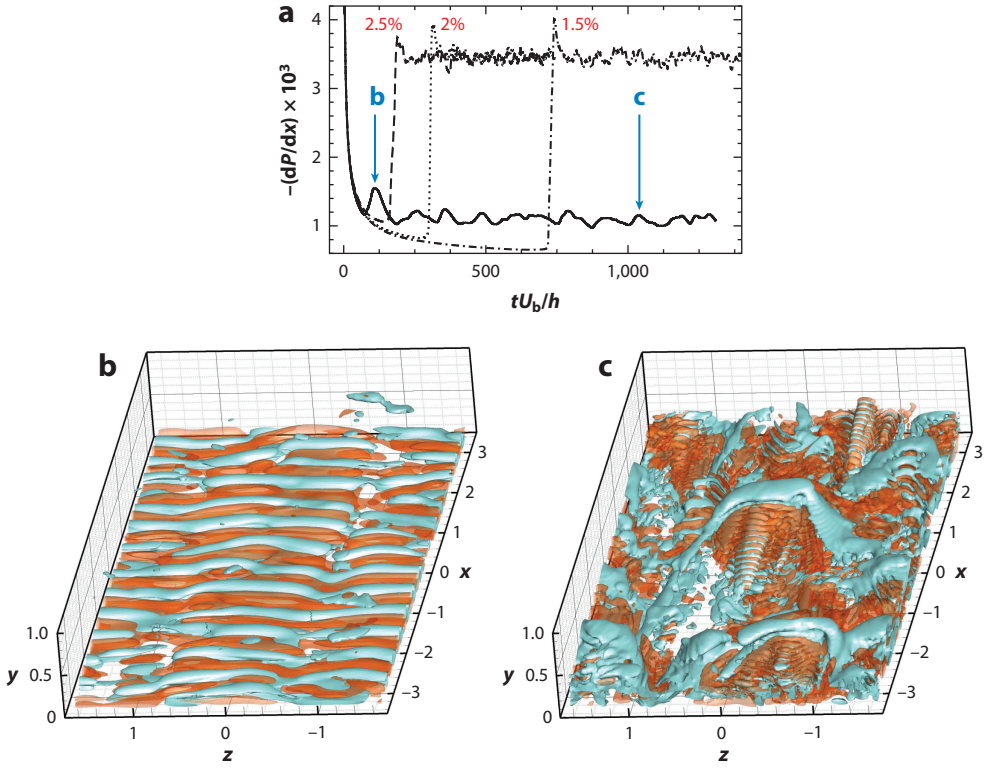

Figure 11

(*a*) Early turbulence numerical experiment of Dubief et al. (2010) in a 3D periodic channel flow at constant mass flow rate. At $tU_b/h = 0$, where $U_b = 1$ is the bulk velocity and $h = 1$ is the half height of the channel, the initial condition consists of a uniform flow in the streamwise direction x, on which a slab of isotropic turbulent perturbations are superimposed in the core region of the flow $-1/2 \leq y/h \leq +1/2$, where y is the wall-normal direction. The initial perturbation is scaled to match a user-defined turbulent intensity (*red*). The dashed, dotted and dash-dotted lines show the evolution of pressure gradient for the flow without polymers. The solid line is the result of a polymer flow for an initial perturbation with turbulent intensity of 1.5%. (*b*,*c*) The structure of positive (*blue*) and negative (*orange*) isosurfaces of the second invariant Q of the velocity gradient tensor, at the beginning of the transition and in the fully developed regime, respectively. These times are highlighted by blue arrows in panel *a*. The flow direction is from $x = -\pi$ to $x = \pi$. The Reynolds number is $Re_b = U_b h/\nu = 5{,}000$. Figure adapted from Dubief et al. (2010) with permission.

they manage to excite instabilities at the wall before the core turbulence reaches it. The flow with additives was subjected to initial perturbations with weak turbulent intensity u'/U_b, where u' is the root mean square of the velocity fluctuations, which indeed triggered a departure from the laminar state much sooner than the Newtonian flow with same, or higher, initial turbulent intensity, as shown in **Figure 11*a***.

Q: second invariant of the velocity gradient tensor

Using the isosurfaces of second invariant $Q = -(1/2)\partial_j u_i \partial_i u_j$ of the velocity gradient tensor $\partial_j u_i$ to track the emergence of vortices revealed an unexpected spanwise organization of positive and negative isosurfaces of Q. Hunt et al. (1988) first proposed to use positive regions of Q for vortex identification. In incompressible flows, Q is proportional to the Laplacian of pressure, $\partial_i \partial_i p = 2Q$, and an enclosed region of positive Q is also a region of minimum pressure. The Q-criterion is one of the most popular vortex identification methods; however, much like other methods, it is not objective: A positive region of Q is not necessarily a vortex, and a proper vortex identification method requires a subjective threshold Q_{th} above which closed isosurfaces of $Q \geq Q_{th}$ may be verified to exhibit the characteristic dynamics of vortices, such as swirling local streamlines (Dubief & Delcayre 2000). In the case of EIT shown in **Figure 11*b***, positive Q-isosurfaces do not qualify as vortices inducing spiraling patterns in the velocity vectors in any local convection reference frame. Given that Q may also be expressed as the difference between the square of the norm of the rotation and strain tensors, the train of positive and negative Q-isosurfaces may also be interpreted as regions of local rotation $Q > 0$ and dissipation of turbulent kinetic energy $Q < 0$.

In the fully developed flow, **Figure 11*c*** is representative of a high-friction drag event with a few visible hairpin vortices, a typical large coherent vortex observed in transitional flows and intermittently in fully turbulent flows. The shape of the observed hairpin vortices is different from Newtonian vortices due to viscoelastic stress. The hoop stress makes the core of vortices look more angular. But the most striking difference with transitional or fully turbulent Newtonian wall-bounded turbulence is the presence of trains of alternating sign, cylindrical Q structures similar to those at the onset of early turbulence. These structures are found in the wake of the head of hairpin vortices and in streaks. During low-drag events (not shown in **Figure 11**), the structure of Q is predominantly aligned in the spanwise direction. The spanwise length scale of these structures is that of the wavelength of the streak instability influenced by the viscoelasticity of the flow (Dubief et al. 2013).

4.3. Relation Between *Q*-Structures, Pressure, and Polymer Stress

The Q-structures have been shown to be attached to the sheets of high polymer stress and their relation to pressure and polymer stress has been discussed by Dubief et al. (2013), Terrapon et al. (2015), and Sid et al. (2018). The key equation relating Q, pressure, and viscoelastic stress is derived by applying the divergence operator to Equation 2 and using the divergence-free property of the velocity field (Equation 1). This equation is also known as the Poisson equation for pressure:

$$\partial_i \partial_i p = -\partial_i u_j \partial_j u_i + \frac{1-\beta}{Re} \partial_i \partial_j T_{ij} = 2Q + \frac{1-\beta}{Re} \partial_i \partial_j T_{ij} \,. \qquad 7.$$

In strong EIT flows, the contribution of the viscoelastic stress term dominates that of $2Q$, which is the contribution of the advection term. Interestingly, this equation simplifies in Stokes flows with the Laplacian of pressure equating the divergence of the divergence of polymer stress. If EIT and ET are to be dynamically related, and we anticipate that they are, the universal dynamics is likely to be hidden in Equation 7. Terrapon et al. (2015) studied the pressure by splitting its inertial and elastic contribution and further analyzing the latter in terms of rapid and slow parts. The elastic rapid part dominates, causing a redistribution of energy from the streamwise component to

other components. Due to the elliptic nature of Equation 7, the cylindrical nature of *Q*-structures, reminiscent of Kelvin–Helmholtz instability, should not be a surprise. The seed of the *Q*-structures appears to be the undulations in the sheets of high N_1 identified in **Figure 10*a*,*b***. These trains do not exist around the sheets forming the steady arrowhead structure in 2D flows (**Figure 10*g***).

TKE: turbulent kinetic energy

TEE: turbulent elastic energy

4.4. Perspectives on Self-Sustaining Cycle for Elasto-Inertial Turbulence

The polymer and flow structures of EIT reveal a very different dynamical picture than turbulent or even transitional Newtonian flows. Wall-bounded turbulent flows are governed by a self-sustaining cycle of interactions between mean shear and coherent structures arising from well-understood instabilities (Waleffe 1997, Jiménez & Pinelli 1999). A fundamental difference between the self-sustaining process of Newtonian wall-turbulence and that of EIT is in the energy transfer between scales. In Newtonian turbulence, the energy flows from large to small scales through the well-known Kolmogorov cascade. In EIT, or at least in simulated EIT, the high–Schmidt number effect discussed by Sid et al. (2018) and in Section 2.2, as well as the analysis of energy transfer between turbulent kinetic energy (TKE) and turbulent elastic energy (TEE) conducted by Dubief et al. (2022), shows that the energy transfer from TEE to TKE is from small to larger scales and that this energy transfer most likely sustains chaotic pressure and velocity fluctuations, which in turn sustain the existence of N_1 sheets and their undulations (Dubief et al. 2013, Terrapon et al. 2015).

The understanding and modeling of EIT requires the derivation of a self-sustaining cycle that ties together the recent developments in stability analysis and the study of flow and polymer coherent structures. Zhang et al. (2021a, 2022) derived a self-sustaining process on the basis of the turbulent kinetic and elastic energy budget, demonstrating the validity of earlier observations that EIT is fundamentally different from IT (Dubief et al. 2013, Terrapon et al. 2015). The effort of Zhang et al. focused on subcritical, critical, and supercritical Reynolds numbers (yet still low from the perspective of IT), and their statistical analysis could pave the way to turbulent models of EIT, which are currently lacking.

Of equal importance, efforts should be continued to establish a parallel between the dynamics observed in simulations and in experiments. At the moment, the similarity between simulations and experiments is based on statistics of drag and fluctuations of pressure and velocity, not on coherent structures.

5. ELASTO-INERTIAL TURBULENCE AND ITS RELATION TO THE MAXIMUM DRAG REDUCTION ASYMPTOTE

The MDR asymptote (see **Figure 1*a***) is one of the most intriguing and least well understood aspects of polymer drag reduction. As we discussed in Section 1.1, its interpretation as a marginal state of ordinary turbulence cannot readily explain how this state becomes stabilized and why higher polymer concentrations fall short of relaminarizing the flow. Samanta et al.'s (2013) finding that the elasto-inertial instability (**Figure 3**) can be traced to higher Reynolds numbers and to parameter values well inside the polymer drag reduction regime has given rise to an alternative interpretation of MDR. Based on what is known about the nature of the elasto-inertial instability, it is plausible to assume that EIT will unavoidably arise as the shear or polymer concentration is increased (i.e., increasing Weissenberg number). This on its own will necessarily prevent flows from being laminar at sufficiently large *Wi*. Samanta et al. also observed that starting from EIT at low Reynolds numbers, the MDR asymptote is directly approached as *Re* is increased without the typical signatures of Newtonian turbulence transition (i.e., neither spatiotemporal intermittency nor hysteresis were detected). Based on these observations the authors suggested that the MDR

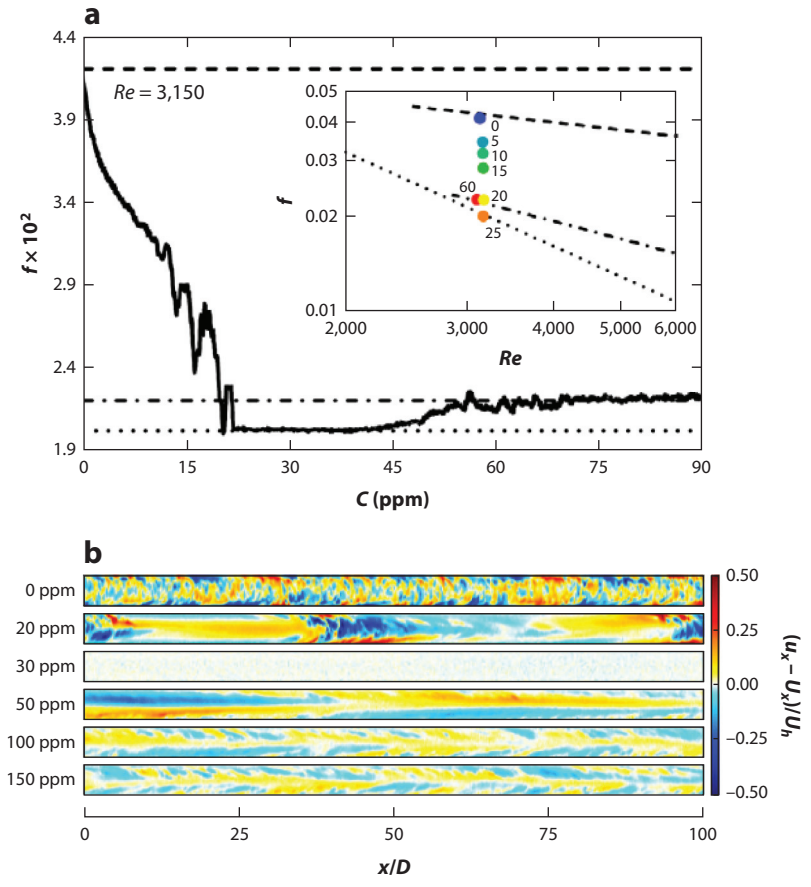

Figure 12

Starting from a fully turbulent flow at Reynolds number $Re = 3{,}150$, Choueiri et al. (2018) showed that (*a*) for increasing polymer concentration C the friction factor decreases past the maximum drag reduction (MDR) limit and reaches the laminar Hagen–Poiseuille level (*dotted line*). As the polymer concentration is further increased the flow eventually destabilizes and the drag increases to the MDR level (*dash-dotted line*). (*b*) The deviation of streamwise velocity fluctuations with respect to the mean, $(u_x - U_x)/U_b$ for $Re = 3{,}150$ and various polymer concentrations. Figure adapted from Choueiri et al. (2018) with permission; copyright 2018 American Physical Society.

asymptote may correspond to the characteristic friction scaling of EIT and, hence, that the MDR limit may be entirely dominated by EIT.

Subsequently, Choueiri et al. (2018) demonstrated that for selected parameter values the addition of polymers can, unexpectedly, fully relaminarize turbulence (**Figure 12**). Starting from a fully turbulent Newtonian flow and keeping Re constant ($Re = 3{,}150$), they increased the polymer concentration and observed an inverse transition. Here turbulence at first reduced in amplitude but then, despite the large Reynolds number value, laminar gaps appeared and the flow became spatiotemporally intermittent. While initially the turbulent regions took the form of expanding slugs, for larger polymer concentration turbulence reduced to transitional puffs and eventually the flow fully relaminarized. Yet higher polymer concentrations led to an instability of the laminar flow, and the weakly fluctuating flow was found to have a friction factor comparable to the MDR asymptote. This observation suggests that, at least for these specific parameters, the so-called MDR state is

not dynamically connected to Newtonian turbulence and results entirely from EIT. The relaminarization also shows that for selected parameters, despite its name, polymers can reduce the drag beyond the MDR limit. Complete relaminarization at moderate Reynolds numbers has subsequently been confirmed in experiments (Chandra et al. 2020) and has equally been demonstrated in FENE-P simulations of pipe and channel flow (Lopez et al. 2019, Shekar et al. 2019). In addition to confirming the reverse transition, relaminarization, and subsequent onset of EIT, Lopez et al. (2019) carried out simulations in pipes of different lengths and could also show that hibernation events (i.e., quiescent time intervals) that are found in short pipes (Xi & Graham 2010) correspond to spatiotemporal intermittency (and, hence, a reverse transition to puffs and slugs) in long pipes. Hence, hibernation is a signature of relaminarization and is encountered prior to the approach to the MDR asymptote. While all these observations confirm the connection between the MDR limit and EIT, these findings cannot clarify if the asymptotic MDR state is solely determined by EIT or if, particularly at higher *Re*, MDR corresponds to a mixed state comprising EIT and Newtonian turbulence. In order to elucidate this point, Choueiri et al. (2021) measured flow fields in experiments and compared structures of EIT at Reynolds numbers where Newtonian turbulence does not exist ($Re \leq 1{,}000$) to MDR at $Re = 10{,}000$. As shown in **Figure 11** at least qualitatively, flow structures resemble each other and look clearly different from turbulence in a Newtonian fluid. Another recent study (Zhu & Xi 2021) questioned whether the MDR state is really asymptotic. In their computations these authors noted that, although the friction level saturates, the dynamics of the instantaneous friction factor values continue to change with increasing Weissenberg numbers. Yet another numerical study (Zhang et al. 2021b, 2022) observed saturation at high Weissenberg numbers. An original contribution of the latter study is the decomposition of the skin friction in terms of viscous, Reynolds (IT), linear elastic, and nonlinear elastic (EIT) contributions, showing that EIT dominates at high *Wi*. More studies are needed in the high-*Wi*, high-*L* parameter space to settle the understanding of the role of EIT in MDR. Of critical importance is that the future studies should focus on finer resolutions than the two numerical studies discussed here in order to assess the possible role of small scales of EIT on MDR.

SUMMARY POINTS

1. The elasto-inertial instability arises for increasing Weissenberg number *Wi* in viscoelastic pipe and channel flows. Not only is elasto-inertial turbulence (EIT) encountered at low Reynolds number *Re* (early turbulence), but EIT structures persist across a wide parameter regime and, in particular, are found in the maximum drag reduction (MDR) limit.
2. The high-dimensional parameter space offers several pathways to EIT. While the recently discovered center mode linear instability provides a possible supercritical route, the transition is likely subcritical in a large part of the parameter space, with new elastically driven attractors, such as the arrowhead in 2D or other ones in 3D, as underlying backbones in a dynamical system perspective.
3. The fundamental instabilities sustaining EIT over a large range of *Re* are 2D; 3D structures resemble 2D structures with a three-dimensionality caused by their interactions with nonlinear Newtonian instabilities like streaks or vortices.
4. The numerical simulation of EIT requires patience: The large-scale dynamics is slow and requires many flow times to achieve statistically steady-state. The smallest scales of

the polymer dynamics however necessitate high resolution and small time steps due to the stiffness of the polymer model transport equation.

5. EIT is likely connected to elastic turbulence (ET) and MDR.

FUTURE ISSUES

1. A direct link should be established between theory, simulations, and experiments, specifically with respect to the experimental prediction of instability thresholds and the qualitative and quantitative comparison of flow structures observed in experiments and simulations.
2. Is EIT simply an inertial version of ET or does inertia play a more fundamental role?
3. Are the flow structures and properties in the MDR limit fully determined by EIT or do Newtonian-type vortices and streaks and the underlying sustaining cycle persist at some level?
4. The transformation of the center mode that arises from the linear instability to the near-wall inclined structures, which is characteristic of EIT at larger *Wi*, is currently not understood.
5. Unraveling the self-sustaining mechanism of EIT not only is necessary to derive the theory and modeling of EIT but also may help identify fundamental dynamics shared with ET.
6. New algorithms are needed to accelerate simulations of EIT.

DISCLOSURE STATEMENT

The authors are not aware of any biases that might be perceived as affecting the objectivity of this review.

ACKNOWLEDGMENTS

Part of the material presented here is based upon work supported by the National Science Foundation CBET (Chemical, Bioengineering, Environmental and Transport Systems) award 1805636 (to Y.D.), the Binational Science Foundation award 2016145 (to Y.D. and Victor Steinberg), a FRIA (Fund for Research Training in Industry and Agriculture) grant of the Belgian F.R.S.-FNRS (National Fund for Scientific Research) (to V.E.T.), the Marie Curie FP7 Career Integration grant PCIG10-GA-2011-304073 (to V.E.T.), and the *Fonds spéciaux pour la recherche* grant C-13/19 of the University of Liege (to V.E.T.). Computational resources have been provided by the *Consortium des Équipements de Calcul Intensif* (CECI) funded by the Belgian F.R.S.-FNRS, the Vermont Advanced Computing Center (VACC), the Partnership for Advanced Computing in Europe (PRACE), and the Tier-1 supercomputer of the *Fédération Wallonie-Bruxelles* funded by the Walloon Region (grant agreement 117545).

LITERATURE CITED

Agarwal A, Brandt L, Zaki TA. 2014. Linear and nonlinear evolution of a localized disturbance in polymeric channel flow. *J. Fluid Mech.* 760:278–303

Alves M, Oliveira P, Pinho F. 2021. Numerical methods for viscoelastic fluid flows. *Annu. Rev. Fluid Mech.* 53:509–41
Avila K, Moxey D, de Lozar A, Avila M, Barkley D, Hof B. 2011. The onset of turbulence in pipe flow. *Science* 333(6039):192–96
Avila M, Barkley D, Hof B. 2023. Transition to turbulence in pipe flow. *Annu. Rev. Fluid Mech.* 55:575–602
Barnes HA, Hutton JF, Walters K. 1989. *An Introduction to Rheology*, Vol. 3. Amsterdam: Elsevier
Batchelor GK. 1959. Small-scale variation of convected quantities like temperature in turbulent fluid. Part 1. General discussion and the case of small conductivity. *J. Fluid Mech.* 5(1):113–33
Batchelor GK, Howells ID, Townsend AA. 1959. Small-scale variation of convected quantities like temperature in turbulent fluid. Part 2. The case of large conductivity. *J. Fluid Mech.* 5(1):134–39
Berti S, Bistagnino A, Boffetta G, Celani A, Musacchio S. 2008. Two-dimensional elastic turbulence. *Phys. Rev. E* 77(5):055306
Bird R, Armstrong R, Hassager O. 1987. *Dynamics of Polymeric Liquids*, Vol. 2: *Kinetic Theory*. New York: Wiley-Intersci.
Buza G, Page J, Kerswell RR. 2022. Weakly nonlinear analysis of the viscoelastic instability in channel flow for finite and vanishing Reynolds numbers. *J. Fluid Mech.* 940:A11
Chandra B, Shankar V, Das D. 2018. Onset of transition in the flow of polymer solutions through microtubes. *J. Fluid Mech.* 844:1052–83
Chandra B, Shankar V, Das D. 2020. Early transition, relaminarization and drag reduction in the flow of polymer solutions through microtubes. *J. Fluid Mech.* 885:A47
Chaudhary I, Garg P, Shankar V, Subramanian G. 2019. Elasto-inertial wall mode instabilities in viscoelastic plane Poiseuille flow. *J. Fluid Mech.* 881:119–63
Chaudhary I, Garg P, Subramanian G, Shankar V. 2021. Linear instability of viscoelastic pipe flow. *J. Fluid Mech.* 908:A11
Choueiri GH, Lopez JM, Hof B. 2018. Exceeding the asymptotic limit of polymer drag reduction. *Phys. Rev. Lett.* 120(12):124501
Choueiri GH, Lopez JM, Varshney A, Sankar S, Hof B. 2021. Experimental observation of the origin and structure of elastoinertial turbulence. *PNAS* 118(45):e2102350118
Doering CR, Eckhardt B, Schumacher J. 2006. Failure of energy stability in Oldroyd-B fluids at arbitrarily low Reynolds numbers. *J. Non-Newton. Fluid Mech.* 135(2–3):92–96
Dong M, Zhang M. 2022. Asymptotic study of linear instability in a viscoelastic pipe flow. *J. Fluid Mech.* 935:A28
Dubief Y, Delcayre F. 2000. On coherent-vortex identification in turbulence. *J. Turbul.* 1:N11
Dubief Y, Page J, Kerswell RR, Terrapon VE, Steinberg V. 2022. A first coherent structure in elasto-inertial turbulence. *Phys. Rev. Fluids* 7:073301
Dubief Y, Terrapon V, White C, Shaqfeh E, Moin P, Lele S. 2005. New answers on the interaction between polymers and vortices in turbulent flows. *Flow Turbul. Combust.* 74(4):311–29
Dubief Y, Terrapon VE, Soria J. 2013. On the mechanism of elasto-inertial turbulence. *Phys. Fluids* 25(11):110817
Dubief Y, White C. 2011. *Elastic turbulence in high Reynolds number polymer drag reduced flows*. Abstract presented at APS Division of Fluid Dynamics Meeting, Baltimore, MD, Nov. 20–22, Abstr. M8–002
Dubief Y, White CM, Shaqfeh ESG, Terrapon VE. 2010. Polymer maximum drag reduction: a unique transitional state. In *Annual Research Briefs*, pp. 395–404. Stanford, CA: Cent. Turbul. Res.
Eckhardt B, Schneider TM, Hof B, Westerweel J. 2007. Turbulence transition in pipe flow. *Annu. Rev. Fluid Mech.* 39:447–68
Fattal R, Kupferman R. 2005. Time-dependent simulation of viscoelastic flows at high Weissenberg number using the log-conformation representation. *J. Non-Newton. Fluid Mech.* 126:23–37
Forame PC, Hansen RJ, Little RC. 1972. Observations of early turbulence in the pipe flow of drag reducing polymer solutions. *AIChE J.* 18:213–17
Garg P, Chaudhary I, Khalid M, Shankar V, Subramanian G. 2018. Viscoelastic pipe flow is linearly unstable. *Phys. Rev. Lett.* 121(2):024502
Goldstein M, Hultgren LS. 1989. Boundary-layer receptivity to long-wave free-stream disturbances. *Annu. Rev. Fluid Mech.* 21:137–66

Gorodtsov V, Leonov A. 1967. On a linear instability of a plane parallel Couette flow of viscoelastic fluid. *J. Appl. Math. Mech.* 31(2):310–19

Graham MD. 2014. Drag reduction and the dynamics of turbulence in simple and complex fluids. *Phys. Fluids* 26(10):101301

Graham MD, Floryan D. 2021. Exact coherent states and the nonlinear dynamics of wall-bounded turbulent flows. *Annu. Rev. Fluid Mech.* 53:227–53

Grillet AM, Bogaerds AC, Peters GW, Baaijens FP. 2002. Stability analysis of constitutive equations for polymer melts in viscometric flows. *J. Non-Newton. Fluid Mech.* 103(2–3):221–50

Groisman A, Steinberg V. 2000. Elastic turbulence in a polymer solution flow. *Nature* 405(6782):53–55

Hameduddin I, Gayme DF, Zaki TA. 2019. Perturbative expansions of the conformation tensor in viscoelastic flows. *J. Fluid Mech.* 858:377–406

Hameduddin I, Meneveau C, Zaki TA, Gayme DF. 2018. Geometric decomposition of the conformation tensor in viscoelastic turbulence. *J. Fluid Mech.* 842:395–427

Hariharan G, Jovanović MR, Kumar S. 2018. Amplification of localized body forces in channel flows of viscoelastic fluids. *J. Non-Newton. Fluid Mech.* 260:40–53

Ho TC, Denn MM. 1977. Stability of plane Poiseuille flow of a highly elastic liquid. *J. Non-Newton. Fluid Mech.* 3(2):179–95

Hoda N, Jovanović MR, Kumar S. 2008. Energy amplification in channel flows of viscoelastic fluids. *J. Fluid Mech.* 601:407–24

Hoda N, Jovanović MR, Kumar S. 2009. Frequency responses of streamwise-constant perturbations in channel flows of Oldroyd-B fluids. *J. Fluid Mech.* 625:411–34

Hof B, De Lozar A, Kuik DJ, Westerweel J. 2008. Repeller or attractor? Selecting the dynamical model for the onset of turbulence in pipe flow. *Phys. Rev. Lett.* 101(21):214501

Hof B, Samanta D, Wagner C. 2011. *The maximum drag reduction asymptote*. Abstract presented at APS Division of Fluid Dynamics Meeting, Baltimore, MD, Nov. 20–22, Abstr. M8-005

Hof B, Westerweel J, Schneider TM, Eckhardt B. 2006. Finite lifetime of turbulence in shear flows. *Nature* 443(7107):59–62

Hoyt J. 1977. Laminar-turbulent transition in polymer solutions. *Nature* 270:508–9

Hunt JC, Wray AA, Moin P. 1988. Eddies, streams, and convergence zones in turbulent flows. In *Studying Turbulence Using Numerical Simulation Databases, II: Proceedings of the 1988 Summer Program*, pp. 193–208. Stanford, CA: Cent. Turbul. Res.

Jha NK, Steinberg V. 2021. Elastically driven Kelvin–Helmholtz-like instability in straight channel flow. *PNAS* 118(34):e2105211118

Jiménez J. 1994. On the structure and control of near wall turbulence. *Phys. Fluids* 6(2):944–53

Jiménez J, Flores O, Garca-Villalba M. 2001. The large-scale organization of autonomous turbulent wall regions. In *Annual Research Briefs 2001*, pp. 317–27. Stanford, CA: Cent. Turbul. Res.

Jiménez J, Moin P. 1991. The minimal flow unit in near-wall turbulence. *J. Fluid Mech.* 225:213–40

Jiménez J, Pinelli A. 1999. The autonomous cycle of near-wall turbulence. *J. Fluid Mech.* 389:335–59

Jovanović MR, Kumar S. 2009. Variance amplification in channel flows of strongly elastic polymer solutions. In *2009 American Control Conference*, pp. 842–47. New York: IEEE

Jovanović MR, Kumar S. 2010. Transient growth without inertia. *Phys. Fluids* 22(2):023101

Jovanović MR, Kumar S. 2011. Nonmodal amplification of stochastic disturbances in strongly elastic channel flows. *J. Non-Newton. Fluid Mech.* 166(14–15):755–78

Kerswell RR. 2005. Recent progress in understanding the transition to turbulence in a pipe. *Nonlinearity* 18(6):R17–44

Khalid M, Chaudhary I, Garg P, Shankar V, Subramanian G. 2021a. The centre-mode instability of viscoelastic plane Poiseuille flow. *J. Fluid Mech.* 915:A43

Khalid M, Shankar V, Subramanian G. 2021b. Continuous pathway between the elasto-inertial and elastic turbulent states in viscoelastic channel flow. *Phys. Rev. Lett.* 127(13):134502

Kim J, Moin P, Moser R. 1987. Turbulence statistics in fully developed channel flow at low Reynolds number. *J. Fluid Mech.* 177:133–66

Larson RG. 1992. Instabilities in viscoelastic flows. *Rheol. Acta* 31(3):213–63

Larson RG, Shaqfeh E, Muller S. 1990. A purely elastic instability in Taylor–Couette flow. *J. Fluid Mech.* 218(1):573–600

Layec Y, Layec-Raphalen MN. 1983. Instability of dilute poly (ethylene-oxide) solutions. *J. Phys. Lett.* 44(3):121–28

Li CF, Sureshkumar R, Khomami B. 2006. Influence of rheological parameters on polymer induced turbulent drag reduction. *J. Non-Newton. Fluid Mech.* 140(1–3):23–40

Li W, Graham M. 2007. Polymer induced drag reduction in exact coherent structures of plane Poiseuille flow. *Phys. Fluids* 19:083101

Little RC, Hansen R, Hunston D, Kim O, Patterson R, Ting R. 1975. The drag reduction phenomenon. Observed characteristics, improved agents, and proposed mechanisms. *Ind. Eng. Chem. Fundamen.* 14(4):283–96

Little RC, Wiegard M. 1970. Drag reduction and structural turbulence in flowing polyox solutions. *J. Appl. Polymer Sci.* 14(2):409–19

Lopez JM, Choueiri GH, Hof B. 2019. Dynamics of viscoelastic pipe flow at low Reynolds numbers in the maximum drag reduction limit. *J. Fluid Mech.* 874:699–719

Lumley J. 1969. Drag reduction by additives. *Ann. Rev. Fluid Mech.* 1:367–84

McKinley GH, Byars JA, Brown RA, Armstrong RC. 1991. Observations on the elastic instability in cone-and-plate and parallel-plate flows of a polyisobutylene Boger fluid. *J. Non-Newton. Fluid Mech.* 40(2):201–29

Meulenbroek B, Storm C, Morozov AN, van Saarloos W. 2004. Weakly nonlinear subcritical instability of visco-elastic Poiseuille flow. *J. Non-Newton. Fluid Mech.* 116(2–3):235–68

Min T, Yoo JY, Choi H. 2001. Effect of spatial discretization schemes on numerical solutions of viscoelastic fluid flows. *J. Non-Newton. Fluid Mech.* 100(1–3):27–47

Morozov AN, van Saarloos W. 2005. Subcritical finite-amplitude solutions for plane Couette flow of viscoelastic fluids. *Phys. Rev. Lett.* 95(2):024501

Morozov AN, van Saarloos W. 2007. An introductory essay on subcritical instabilities and the transition to turbulence in visco-elastic parallel shear flows. *Phys. Rep.* 447(3–6):112–43

Morozov AN, van Saarloos W. 2019. Subcritical instabilities in plane Poiseuille flow of an Oldroyd-B fluid. *J. Stat. Phys.* 175(3–4):554–77

Mukund V, Hof B. 2018. The critical point of the transition to turbulence in pipe flow. *J. Fluid Mech.* 839:76–94

Orlandi P, Jiménez J. 1994. On the generation of turbulent wall friction. *Phys. Fluids* 6(2):634–41

Ostwald W, Auerbach R. 1926. Ueber die Viskosität kolloider Lösungen im Struktur-, Laminar- und Turbulenzgebiet. *Kolloid-Zeitschrift* 38(3):261–280

Page J, Dubief Y, Kerswell RR. 2020. Exact traveling wave solutions in viscoelastic channel flow. *Phys. Rev. Lett.* 125(15):154501

Page J, Zaki TA. 2014. Streak evolution in viscoelastic Couette flow. *J. Fluid Mech.* 742:520–51

Page J, Zaki TA. 2015. The dynamics of spanwise vorticity perturbations in homogeneous viscoelastic shear flow. *J. Fluid Mech.* 777:327–63

Páll S, Zhmurov A, Bauer P, Abraham M, Lundborg M, et al. 2020. Heterogeneous parallelization and acceleration of molecular dynamics simulations in GROMACS. *J. Chem. Phys.* 153(13):134110

Pan L, Morozov A, Wagner C, Arratia P. 2013. Nonlinear elastic instability in channel flows at low Reynolds numbers. *Phys. Rev. Lett.* 110(17):174502

Porteous KC, Denn MM. 1972. Linear stability of plane Poiseuille flow of viscoelastic liquids. *Trans. Soc. Rheol.* 16(2):295–308

Ptasinski P, Boersma B, Nieuwstadt F, Hulsen M, Van den Brule B, Hunt J. 2003. Turbulent channel flow near maximum drag reduction: simulations, experiments and mechanisms. *J. Fluid Mech.* 490:251–91

Qin B, Arratia PE. 2017. Characterizing elastic turbulence in channel flows at low Reynolds number. *Phys. Rev. Fluids* 2(8):083302

Ram A, Tamir A. 1964. Structural turbulence in polymer solutions. *J. Appl. Polymer Sci.* 8(6):2751–62

Reiner M. 1926a. Ueber die Strömung einer elastischen Flüssigkeit durch eine Kapillare. *Kolloid-Zeitschrift* 39(1):80–87

Reiner M. 1926b. Zur Theorie der "Strukturturbulenz." *Kolloid-Zeitschrift* 39(4):314–15

Reynolds O. 1883. An experimental investigation of the circumstances which determine whether the motion of water shall be direct or sinuous, and of the law of resistance in parallel channels. *Philos. Trans. R. Soc. Lond.* 174:935–82

Samanta D, Dubief Y, Holzner M, Schäfer C, Morozov AN, et al. 2013. Elasto-inertial turbulence. *PNAS* 110(26):10557–62

Sánchez HAC, Jovanović MR, Kumar S, Morozov A, Shankar V, et al. 2022. Understanding viscoelastic flow instabilities: Oldroyd-B and beyond. *J. Non-Newton. Fluid Mech.* 302:104472

Schmid PJ. 2007. Nonmodal stability theory. *Annu. Rev. Fluid Mech.* 39:129–62

Schmid PJ, Henningson D. 2000. *Stability and Transition in Shear Flows*. New York: Springer

Shaqfeh E. 1996. Purely elastic instabilities in viscometric flows. *Annu. Rev. Fluid Mech.* 28:129–85

Shekar A, McMullen RM, McKeon BJ, Graham MD. 2020. Self-sustained elastoinertial Tollmien–Schlichting waves. *J. Fluid Mech.* 897:A3

Shekar A, McMullen RM, McKeon BJ, Graham MD. 2021. Tollmien-Schlichting route to elastoinertial turbulence in channel flow. *Phys. Rev. Fluids* 6(9):093301

Shekar A, McMullen RM, Wang SN, McKeon BJ, Graham MD. 2019. Critical-layer structures and mechanisms in elastoinertial turbulence. *Phys. Rev. Lett.* 122(12):124503

Sid S, Terrapon VE, Dubief Y. 2018. Two-dimensional dynamics of elasto-inertial turbulence and its role in polymer drag reduction. *Phys. Rev. Fluids* 3(1):011301

Srinivas SS, Kumaran V. 2017. Effect of viscoelasticity on the soft-wall transition and turbulence in a microchannel. *J. Fluid Mech.* 812:1076–118

Steinberg V. 2021. Elastic turbulence: an experimental view on inertialess random flow. *Annu. Rev. Fluid Mech.* 53:27–58

Stone P, Roy A, Larson R, Waleffe F, Graham M. 2004. Polymer drag reduction in exact coherent structures of plane shear flow. *Phys. Fluids* 16:3470

Sureshkumar R, Beris AN. 1995a. Effect of artificial stress diffusivity on the stability of numerical calculations and the flow dynamics of time-dependent viscoelastic flows. *J. Non-Newton. Fluid Mech.* 60(1):53–80

Sureshkumar R, Beris AN. 1995b. Linear stability analysis of viscoelastic Poiseuille flow using an Arnoldi-based orthogonalization algorithm. *J. Non-Newton. Fluid Mech.* 56(2):151–82

Sureshkumar R, Beris AN, Handler R. 1997. Direct numerical simulation of the turbulent channel flow of a polymer solution. *Phys. Fluids* 9:743

Tabor M, De Gennes P. 1986. A cascade theory of drag reduction. *Europhys. Lett.* 2:519–22

Terrapon VE, Dubief Y, Soria J. 2015. On the role of pressure in elasto-inertial turbulence. *J. Turbul.* 16(1):26–43

Thais L, Tejada-Mart AE, Gatski TB, Mompean G, et al. 2011. A massively parallel hybrid scheme for direct numerical simulation of turbulent viscoelastic channel flow. *Comput. Fluids* 43(1):134–42

Toms BA. 1948. Some observations on the flow of linear polymer solutions through straight tubes at large Reynolds numbers. In *Proceedings of the First International Congress on Rheology*, pp. 135–41. Amsterdam: N. Holland

Vaithianathan T, Collins L. 2003. Numerical approach to simulating turbulent flow of a viscoelastic polymer solution. *J. Comput. Phys.* 187:1–21

Vaithianathan T, Robert A, Brasseur JG, Collins LR. 2006. An improved algorithm for simulating three-dimensional, viscoelastic turbulence. *J. Non-Newton. Fluid Mech.* 140(1–3):3–22

Vinogradov GV, Manin VN. 1965. An experimental study of elastic turbulence. *Kolloid-Z. Z. Polym.* 201(2):93–98

Virk P, Mickley H, Smith K. 1970. The ultimate asymptote and mean flow structure in Toms' phenomenon. *J. Appl. Mech* 37:488–93

Waleffe F. 1997. On a self-sustaining process in shear flows. *Phys. Fluids* 9(4):883–900

Waleffe F. 2001. Exact coherent structures in channel flow. *J. Fluid Mech.* 435:93–102

Wan D, Sun G, Zhang M. 2021. Subcritical and supercritical bifurcations in axisymmetric viscoelastic pipe flows. *J. Fluid Mech.* 929:A16

Warholic M, Massah H, Hanratty T. 1999. Influence of drag-reducing polymers on turbulence: effects of Reynolds number concentration and mixing. *Exp. Fluids* 27(5):461–72

Warner HR. 1972. Kinetic theory and rheology of dilute suspensions of finitely extendible dumbbells. *Ind. Eng. Chem. Fundam.* 11(3):379–87

Wen C, Poole RJ, Willis AP, Dennis DJC. 2017. Experimental evidence of symmetry-breaking supercritical transition in pipe flow of shear-thinning fluids. *Phys. Rev. Fluids* 2(3):031901

White C, Mungal M. 2008. Mechanics and prediction of turbulent drag reduction with polymer additives. *Annu. Rev. Fluid Mech.* 40:235–56

Wilson HJ, Renardy M, Renardy Y. 1999. Structure of the spectrum in zero Reynolds number shear flow of the UCM and Oldroyd-B liquids. *J. Non-Newton. Fluid Mech.* 80(2–3):251–68

Xi L. 2019. Turbulent drag reduction by polymer additives: fundamentals and recent advances. *Phys. Fluids* 31:121302

Xi L, Graham M. 2010. Active and hibernating turbulence in minimal channel flow of Newtonian and polymeric fluids. *Phys. Rev. Lett.* 104(21):218301

Zhang M. 2021. Energy growth in subcritical viscoelastic pipe flows. *J. Non-Newton. Fluid Mech.* 294:104581

Zhang M, Lashgari I, Zaki TA, Brandt L. 2013. Linear stability analysis of channel flow of viscoelastic Oldroyd-B and FENE-P fluids. *J. Fluid Mech.* 737:249–79

Zhang WH, Shao QQ, Li YK, Ma Y, Zhang HN, Li FC. 2021a. On the mechanisms of sheet-like extension structures formation and self-sustaining process in elasto-inertial turbulence. *Phys. Fluids* 33(8):085107

Zhang WH, Zhang HN, Li YK, Yu B, Li FC. 2021b. Role of elasto-inertial turbulence in viscoelastic drag-reducing turbulence. *Phys. Fluids* 33(8):081706

Zhang WH, Zhang HN, Wang ZM, Li YK, Yu B, Li FC. 2022. Repicturing viscoelastic drag-reducing turbulence by introducing dynamics of elasto-inertial turbulence. *J. Fluid Mech.* 940:A31

Zhu L, Xi L. 2021. Nonasymptotic elastoinertial turbulence for asymptotic drag reduction. *Phys. Rev. Fluids* 6(1):014601

Annual Review of Fluid Mechanics

Volume 55, 2023

Contents

Flow Computation Pioneer Irmgard Flügge-Lotz (1903–1974)
Jonathan B. Freund 1

Fluid Mechanics in France in the First Half of the Twentieth Century
François Charru 11

New Insights into Turbulent Spots
Xiaohua Wu 45

Self-Propulsion of Chemically Active Droplets
Sébastien Michelin 77

Submesoscale Dynamics in the Upper Ocean
John R. Taylor and Andrew F. Thompson 103

Immersed Boundary Methods: Historical Perspective and Future Outlook
Roberto Verzicco 129

Motion in Stratified Fluids
Rishabh V. More and Arezoo M. Ardekani 157

The Flow Physics of Face Masks
Rajat Mittal, Kenneth Breuer, and Jung Hee Seo 193

Advancing Access to Cutting-Edge Tabletop Science
Michael F. Schatz, Pietro Cicuta, Vernita D. Gordon, Teuta Pilizota, Bruce Rodenborn, Mark D. Shattuck, and Harry L. Swinney 213

Cerebrospinal Fluid Flow
Douglas H. Kelley and John H. Thomas 237

Fluid Dynamics of Polar Vortices on Earth, Mars, and Titan
Darryn W. Waugh 265

Dynamics of Three-Dimensional Shock-Wave/Boundary-Layer Interactions
Datta V. Gaitonde and Michael C. Adler 291

Gas-Liquid Foam Dynamics: From Structural Elements to Continuum Descriptions
Peter S. Stewart and Sascha Hilgenfeldt 323

Recent Developments in Theories of Inhomogeneous and Anisotropic Turbulence
J.B. Marston and S.M. Tobias 351

Icebergs Melting
Claudia Cenedese and Fiamma Straneo 377

The Fluid Mechanics of Deep-Sea Mining
Thomas Peacock and Raphael Ouillon 403

A Perspective on the State of Aerospace Computational Fluid Dynamics Technology
Mori Mani and Andrew J. Dorgan 431

Particle Rafts and Armored Droplets
Suzie Protière 459

Evaporation of Sessile Droplets
Stephen K. Wilson and Hannah-May D'Ambrosio 481

3D Lagrangian Particle Tracking in Fluid Mechanics
Andreas Schröder and Daniel Schanz 511

Linear Flow Analysis Inspired by Mathematical Methods from Quantum Mechanics
Luca Magri, Peter J. Schmid, and Jonas P. Moeck 541

Transition to Turbulence in Pipe Flow
Marc Avila, Dwight Barkley, and Björn Hof 575

Turbulent Rotating Rayleigh–Bénard Convection
Robert E. Ecke and Olga Shishkina 603

Nonidealities in Rotating Detonation Engines
Venkat Raman, Supraj Prakash, and Mirko Gamba 639

Elasto-Inertial Turbulence
Yves Dubief, Vincent E. Terrapon, and Björn Hof 675

Sharp Interface Methods for Simulation and Analysis of Free Surface Flows with Singularities: Breakup and Coalescence
Christopher R. Anthony, Hansol Wee, Vishrut Garg, Sumeet S. Thete, Pritish M. Kamat, Brayden W. Wagoner, Edward D. Wilkes, Patrick K. Notz, Alvin U. Chen, Ronald Suryo, Krishnaraj Sambath, Jayanta C. Panditaratne, Ying-Chih Liao, and Osman A. Basaran 707

Indexes

Cumulative Index of Contributing Authors, Volumes 1–55 749

Cumulative Index of Article Titles, Volumes 1–55 760

Errata

An online log of corrections to *Annual Review of Fluid Mechanics* articles may be found at http://www.annualreviews.org/errata/fluid